Article

An amygdala circuit that suppresses social engagement

https://doi.org/10.1038/s41586-021-03413-6

Received: 29 April 2020

Accepted: 2 March 2021

Published online: 31 March 2021

Check for updates

Jeong-Tae Kwon[1,2], Changhyeon Ryu[1,2,5], Hyeseung Lee[1,2,4,5], Alec Sheffield[1,2], Jingxuan Fan[2], Daniel H. Cho[2], Shivani Bigler[2], Heather A. Sullivan[3], Han Kyung Choe[2], Ian R. Wickersham[3], Myriam Heiman[1,2,4] & Gloria B. Choi[1,2]✉

Innate social behaviours, such as mating and fighting, are fundamental to animal reproduction and survival[1]. However, social engagements can also put an individual at risk[2]. Little is known about the neural mechanisms that enable appropriate risk assessment and the suppression of hazardous social interactions. Here we identify the posteromedial nucleus of the cortical amygdala (COApm) as a locus required for the suppression of male mating when a female mouse is unhealthy. Using anatomical tracing, functional imaging and circuit-level epistatic analyses, we show that suppression of mating with an unhealthy female is mediated by the COApm projections onto the glutamatergic population of the medial amygdalar nucleus (MEA). We further show that the role of the COApm-to-MEA connection in regulating male mating behaviour relies on the neuromodulator thyrotropin-releasing hormone (TRH). TRH is expressed in the COApm, whereas the TRH receptor (TRHR) is found in the postsynaptic MEA glutamatergic neurons. Manipulating neural activity of TRH-expressing neurons in the COApm modulated male mating behaviour. In the MEA, activation of the TRHR pathway by ligand infusion inhibited mating even towards healthy female mice, whereas genetic ablation of TRHR facilitated mating with unhealthy individuals. In summary, we reveal a neural pathway that relies on the neuromodulator TRH to modulate social interactions according to the health status of the reciprocating individual. Individuals must balance the cost of social interactions relative to the benefit, as deficits in the ability to select healthy mates may lead to the spread of disease.

Social behaviours are fundamental for survival—for the individual as well as the species. Social engagements, however, also carry inherent risks, such as contracting pathogens from a sick mate[2]. Thus, the ability to modify innate social behaviours to account for the health status of a partner is essential to minimize potential risks and to enhance survival[3–5]. Innate social behaviours such as mating and aggression[1] are largely thought to be coordinated by developmentally determined neural pathways[6–9]. However, the molecular and neural circuit mechanisms that mediate the adaptive modulation of innate social interactions according to the health of a partner remain unknown.

Males avoid mating with unhealthy females

Mice avoid potentially sick partners. When we presented male mice with a pair of female mice in oestrus, they preferentially mounted those that were intraperitoneally injected with control phosphate-buffered saline (PBS female) over those injected with lipopolysaccharide (LPS female), a component of the cell wall of Gram-negative bacteria that induces an immune state mimicking bacterial infection[10] (Extended Data Fig. 1a, b). No such bias was observed when males were given a choice between two untreated healthy females (Extended Data Fig. 1c). We observed no preference for PBS or LPS females in a three-chamber sociability assay in which females are restrained in wired cups (Extended Data Fig. 1d), suggesting that direct access to the female is probably needed to establish her health status. To further examine the repertoire of male mating behaviours displayed towards unhealthy females, we carried out a single-female assay, in which males were presented either with a PBS or LPS female (Fig. 1a, Extended Data Fig. 1e). Males reduced the amount of anogenital investigation towards LPS females, while maintaining a comparable level of facial investigation (Extended Data Fig. 1f). Notably, the percentage of male mice that mounted LPS females as well as the duration and frequency of mounting bouts were reduced, while the latency to mount LPS females substantially increased (Fig. 1b–e). These observations indicate that males exhibit reduced expression of mating behaviours towards LPS-treated, unhealthy females. Of note, the LPS treatment also induced changes in the repertoire of female behaviours, generally reducing locomotion, as quantified by the total number of cage crossings (Extended Data Fig. 1g–i).

[1]Picower Institute for Learning and Memory, Massachusetts Institute of Technology, Cambridge, MA, USA. [2]Department of Brain and Cognitive Sciences, Massachusetts Institute of Technology, Cambridge, MA, USA. [3]McGovern Institute for Brain Research, Massachusetts Institute of Technology, Cambridge, MA, USA. [4]Broad Institute of MIT and Harvard, Cambridge, MA, USA. [5]These authors contributed equally: Changhyeon Ryu, Hyeseung Lee. ✉e-mail: gbchoi@mit.edu

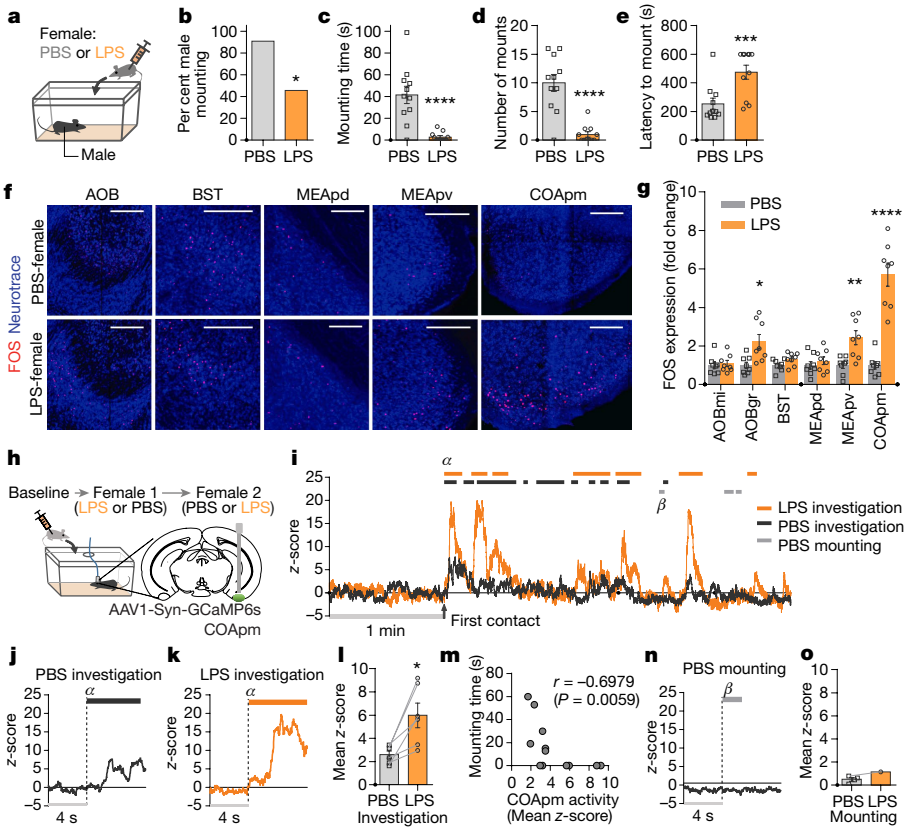

Fig. 1 | COApm is activated by female mice treated with LPS. a–e, Male mounting behaviours towards female mice treated with PBS or LPS. **a**, Experimental setup. **b–e**, Percentage of males engaged in mounting behaviour (**b**), total duration of mounting bouts (**c**), number of mounting attempts (**d**) and latency to the first mounting attempt (**e**) during a 10-min test (PBS, $n = 11$ and LPS, $n = 11$; from 2 independent experiments). **f, g**, Representative images of FOS expression in the vomeronasal pathway after interaction with PBS or LPS females (**f**) and fold change in the number of FOS-expressing neurons normalized to the mean of the PBS female group for each region (**g**) (PBS, $n = 8$ and LPS, $n = 8$; from 2 independent experiments). Scale bars, 200 µm. AOBmi, mitral layer of the accessory olfactory bulb; AOBgr, granular layer of the accessory olfactory bulb; BST, bed nucleus of the stria terminalis; MEApd, posterodorsal part of the medial amygdalar nucleus; MEApv, posteroventral part of the medial amygdalar nucleus. **h–o**, Virus encoding GCaMP6s (AAV_1-Syn-GCaMP6s) was targeted to the COApm for fibre photometry recordings. **h**, Male mice were sequentially presented with a PBS or LPS female mouse in counterbalanced sessions. **i**, Representative trace of COApm bulk fluorescence signal during interactions with the PBS (black and grey) or LPS female (orange). Representative traces (marked as α in (**i**)) with PBS (**j**) or LPS (**k**) females and the average mean *z*-score of the fluorescence (**l**) during the direct investigation of the PBS- or LPS-treated female. **m**, Spearman's correlation between mean *z*-score during investigation and mounting time. Data are obtained from the sessions with PBS and LPS females. **n**, Representative trace (marked as β in (**i**)) (**n**) and the average mean *z*-score of the fluorescence during mounting of the PBS or LPS female (**o**) ($n = 6$ from 3 independent experiments). $^*P < 0.05$, $^{**}P < 0.01$, $^{***}P < 0.001$ and $^{****}P < 0.0001$ calculated by chi-square test of independence (**b**), unpaired two-tailed *t*-test (**c–e**), two-way ANOVA with Sidak's post hoc test (**g**) and paired two-tailed *t*-test (**l**). Data are mean ± s.e.m. *P* values are described in the Supplementary Information.

COApm is activated by unhealthy females

We next carried out experiments using the single-female assay to elucidate the molecular and circuit-level mechanism underlying the suppression of male mating behaviour towards unhealthy LPS females. We reasoned that brain regions in males that have a role in suppressing mating may be specifically activated in the presence of LPS females. Consistent with the role of the accessory olfactory system in recognizing the health of other individuals[11–14], we found that surgically removing the vomeronasal organ impaired active suppression of male mating behaviours towards LPS females (Extended Data Fig. 2a). Thus, using FOS expression as a marker of neural activity, we examined whether the accessory olfactory bulb (AOB) and its direct downstream targets—the BST, MEA, and COApm[15,16] (Extended Data Fig. 2b–d)—are preferentially active when a male is presented with an LPS female compared with a PBS female. We observed the highest fold change in the number of FOS^+ neurons in the COApm and, to a lesser extent, in the AOB and the MEApv (Fig. 1f, g, Extended Data Fig. 2h). To directly monitor COApm neural activity in awake behaving mice, we expressed the genetically encoded fluorescent calcium indicator GCaMP6s and performed fibre photometry (Fig. 1h). Whereas direct investigation of both PBS and LPS females evoked time-locked neural activity in the COApm, the response to LPS females was more pronounced and did not readily habituate when compared with PBS females (Fig. 1i–l, Extended Data Fig. 3a–c). Levels of neural activity in the COApm during investigation, therefore, negatively correlated with the incidence of mounting (Fig. 1m). Notably, the COApm remained silent during mounting (Fig. 1n, o). We did not find any observable difference in COApm neural activity (Extended Data Fig. 3d, e) or males' mounting attempts (Extended Data Fig. 3f–i) towards oestrus versus dioestrus females during a 10-min testing period. However, a higher percentage of oestrus female partners were found with mating plugs 24 h after the testing (Extended Data Fig. 3j), demonstrating their enhanced receptivity compared with dioestrus females. These data collectively indicated that COApm is selectively activated by the unhealthy status of reciprocating females independently of their oestrus phase.

COApm is a direct target of the AOB (Extended Data Fig. 2b–g), suggesting that the suppression of mating behaviours induced by LPS females might depend on non-volatile odorants. We thus used urine and faeces of LPS females as odour sources to test whether odour alone can substitute for an LPS female. Indeed, urine and faeces of LPS females induced a greater number of FOS^+ neurons in the COApm than PBS

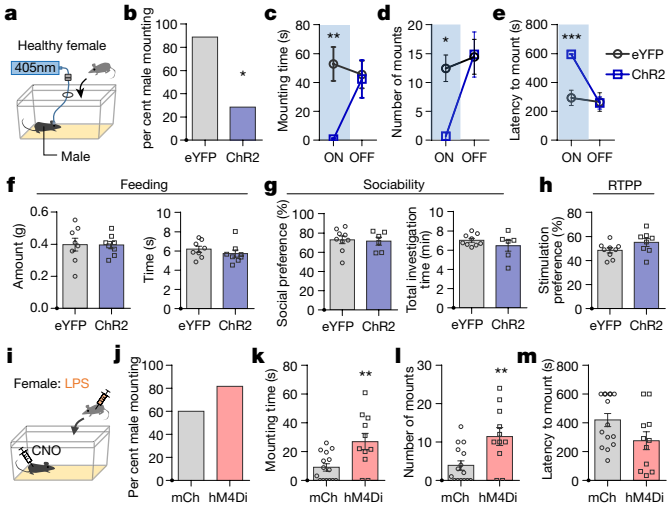

Fig. 2 | COApm mediates suppression of mating behaviours towards unhealthy females. a–e, Male mice expressing enhanced yellow fluorescent protein (eYFP) (AAV_2-hSyn-eYFP) or channelrhodopsin (ChR2) (AAV_2-hSyn-hChR2-eYFP) in COApm were tested for mating behaviours towards healthy female mice in the presence (ON) or absence (OFF) of COApm photoactivation (**a**). Percentage of male mounting (**b**), mounting time (**c**), number of mounts (**d**) and latency to mount (**e**) (eYFP, $n = 9$ and ChR2, $n = 7$; from 2 independent experiments). **f**, Total amount of food eaten and time spent eating, used to assess feeding behaviour during COApm photoactivation (eYFP, $n = 8$ and ChR2, $n = 8$; from 2 independent experiments). **g**, Social preference (time spent investigating a social object/total time spent investigating social and inanimate objects) and total investigation time measured during a sociability test with COApm photoactivation (eYFP, $n = 9$ and ChR2, $n = 6$; from 2 independent experiments). **h**, Stimulation preference (time spent in the compartment where photoactivation occurs/total testing time) during a RTPP test (eYFP, $n = 9$ and ChR2, $n = 8$; from 2 independent experiments). **i–m**, Male mice expressing mCherry (AAV_2-hSyn-mCherry) or inhibitory DREADD (hM4Di) (AAV_2-hSyn-hM4D(G_i)-mCherry) in COApm were injected with clozapine-*N*-oxide (CNO) and tested for mating behaviours towards LPS females (**i**). Percentage of male mounting (**j**), mounting time (**k**), number of mounts (**l**) and latency to mount (**m**) (mCherry, $n = 15$ and hM4Di, $n = 11$; from 3 independent experiments). mCh, mCherry. $^*P < 0.05$, $^{**}P < 0.01$ and $^{***}P < 0.001$ calculated by chi-square test of independence (**b**), two-way repeated measures ANOVA with Bonferroni's post hoc test (**c–e**) and unpaired two-tailed *t*-test (**k**, **l**). Data are mean ± s.e.m. *P* values are described in the Supplementary Information.

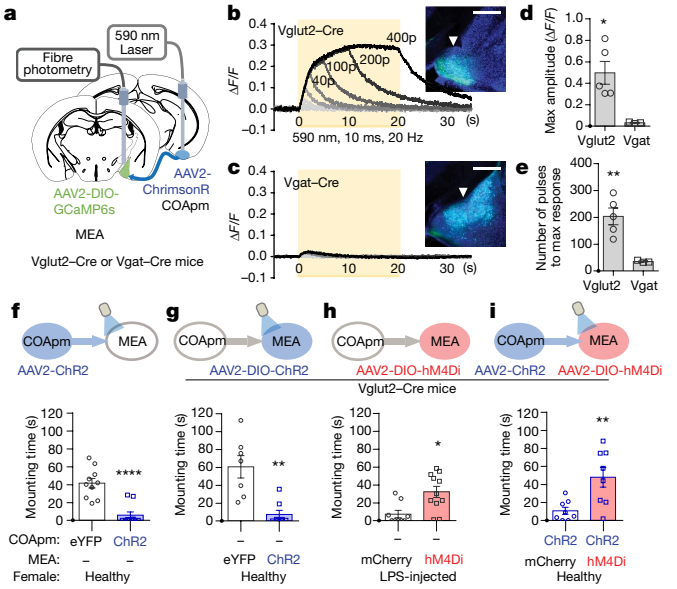

Fig. 3 | COApm projections to MEA-Vglut2$^+$ neurons mediate suppression of mating towards LPS females. a–e, Red-shifted opsin ChrimsonR (AAV_2-hSyn-ChrimsonR-tdTomato) was expressed in COApm, and GCaMP6s was expressed in MEA for fibre photometry analyses. **a**, Bulk fluorescence signal upon COApm photoactivation was measured in either MEA-Vglut2$^+$ or MEA-Vgat$^+$ neurons. Representative traces of changes in fluorescence signal in MEA upon photoactivation of COApm using light trains with 1, 5, 10, 20, 40, 100, 200 or 400 pulses. Images show GCaMP6s expression in MEA-Vglut2$^+$ (**b**) or MEA-Vgat$^+$ (**c**) neurons. Arrowheads indicate the placement of the optic fibre for fibre photometry. **d**, **e**, Maximum (max) amplitude evoked by photoactivation of COApm with 400 pulses of light (**d**) and number of light pulses to reach max amplitude (**e**) (Vglut2-Cre, $n = 5$ and Vgat-Cre, $n = 3$; from 3 independent experiments). Scale bars, 500 µm. **f–i**, Quantification of male mounting behaviours during concurrent manipulation of COApm-MEA axonal projections and MEA-Vglut2$^+$ neurons. Males were wild type (**f**) or Vglut2-Cre (**g–i**). Females were healthy (**f**, **g**, **i**) or injected with LPS (**h**). **f**, Mounting time with photoactivation of COApm-MEA projections (eYFP, $n = 10$ and ChR2, $n = 10$; from 2 independent experiments). **g**, Mounting time with photoactivation of MEA-Vglut2$^+$ neurons (eYFP, $n = 7$ and ChR2, $n = 8$; from 2 independent experiments). **h**, Mounting time towards LPS females with hM4Di inhibition of MEA-Vglut2$^+$ neurons (mCherry, $n = 9$ and hM4Di, $n = 11$; from 2 independent experiments). **i**, Mounting time with concurrent photoactivation of COApm-MEA projections and hM4Di-inhibition of MEA-Vglut2$^+$ neurons (mCherry, $n = 8$ and hM4Di, $n = 8$; from 2 independent experiments). $^*P < 0.05$, $^{**}P < 0.01$ and $^{****}P < 0.0001$ calculated by unpaired two-tailed *t*-test. Data are mean ± s.e.m. *P* values are described in the Supplementary Statistical Information.

odour (Extended Data Fig. 4a–c). We observed similar results using fibre photometry (Extended Data Fig. 4d, e). LPS odour painted on healthy females resulted in a decrease in both mounting and anogenital investigation of otherwise healthy females (Extended Data Fig. 4f–k). Notably, LPS odour suppressed male mating behaviours but did not alter the behaviours of the odour-presenting females (Extended Data Fig. 4l, m), demonstrating that suppression of male sexual behaviours depends largely on the olfactory bouquet of the female rather than the behavioural changes that follow LPS treatment.

COApm suppresses male mating

The observation that COApm preferentially responds to LPS females while remaining silent during mounting suggested that it might be directly involved in suppressing male mating behaviours in the presence of unhealthy partners. Consistent with this notion, optogenetic activation of COApm neurons robustly inhibited mounting even towards healthy females (Fig. 2a–e, Extended Data Fig. 5a). COApm photoactivation, however, did not affect the total investigation time directed towards females (Extended Data Fig. 5b) or the expression of other motivational behaviours, such as feeding and sociability (Fig. 2f, g). Mice also showed neither aversion nor attraction for the side of the chamber where COApm was activated during a real-time place preference test (RTPP) (Fig. 2h). We noted that COApm photoactivation increased self-grooming. However, this increase could at best account for a small fraction of the total reduction in mounting, and the fidelity with which the COApm stimulation induced grooming was low (Extended Data Fig. 5c, d). In accordance with the results from the photoactivation experiments, inhibition of the COApm via bilateral expression of the inhibitory designer receptors exclusively activated by the designer drug (DREADD) hM4Di (Fig. 2i, Extended Data Fig. 5e) significantly increased male mounting behaviour towards LPS females, with male mice exhibiting both heightened duration and frequency of mounting (Fig. 2j–l, Extended Data Fig. 5g–j). The latency to the first mounting attempt showed a trend towards a decrease, although the duration of direct investigation remained unchanged (Fig. 2m, Extended Data Fig. 5f, k). Inhibition of COApm did not affect mounting towards untreated, healthy females regardless of the phase of the oestrus cycle (Extended Data Fig. 5l–u). Together, these results

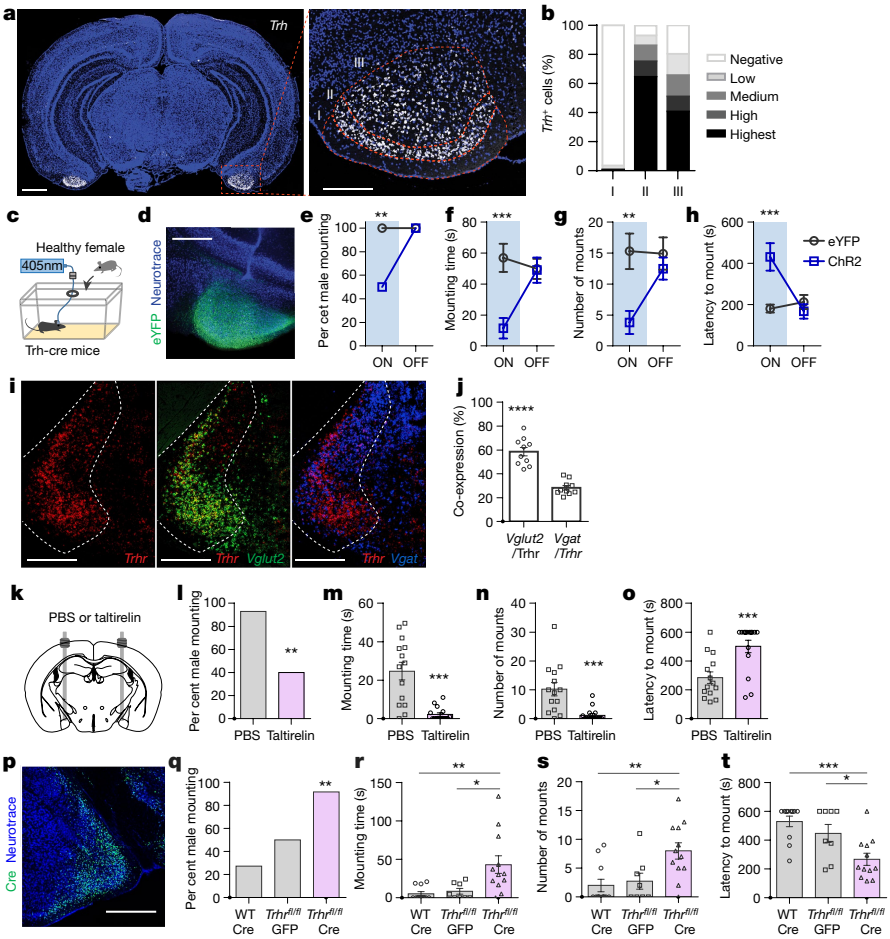

Fig. 4 | Suppression of social behaviours engages COApm-TRH$^+$ neurons. a, **b**, Representative image (**a**) and quantification (**b**) of *Trh* mRNA expression in wild-type mice at anterior-posterior (AP) −2.9 mm according to cortical layers ($n = 13$ sections from 4 mice; from 2 independent experiments). Dotted lines define cortical layers I, II and III. Scale bars, 1 mm (left) and 300 µm (right). **c**–**h**, Trh-Cre male mice expressing eYFP (AAV_2-hSyn-DIO-eYFP) or ChR2 (AAV_2-hSyn-DIO-hChR2-eYFP) in COApm-TRH$^+$ neurons were tested for mating behaviours towards healthy females in the presence (ON) or absence (OFF) of photoactivation (**c**). **d**, Representative image of ChR2 expression in COApm. Scale bar, 500 µm. Percentage of male mounting (**e**), mounting time (**f**), number of mounts (**g**) and latency to mount (**h**) (eYFP, $n = 13$ and ChR2, $n = 10$; from 2 independent experiments). **i**, **j**, Representative images (**i**) and quantification (**j**) of the overlap between cells expressing *Trhr* (red), *Vglut2* (green) and *Vgat* (blue) mRNA in MEA of wild-type mice at AP −1.8 mm ($n = 10$ MEA sections from total 5 mice; from 4 independent experiments). Dotted line indicates MEA. Scale bars, 500 µm. **k**–**o**, The TRH analogue taltirelin was bilaterally injected into MEA (**k**). Percentage of male mounting (**l**), mounting time (**m**), number of mounts (**n**) and latency to mount (**o**) (PBS, $n = 14$ and taltirelin, $n = 15$; from 2 independent experiments). **p**–**t**, Wild-type (WT) or *Trhr*$^{fl/fl}$ male mice expressing GFP (AAV_1-hSyn-GFP) or Cre (AAV_1-Syn-Cre) in the MEA were tested for mating behaviours towards LPS females. Representative image of Cre expression in MEA (**p**). Percentage of male mounting (**q**), mounting time (**r**), number of mounts (**s**) and latency to mount (**t**) (WT-Cre, $n = 11$; *Trhr*$^{fl/fl}$-eYFP, $n = 8$ and *Trhr*$^{fl/fl}$-Cre, $n = 12$; from 2 independent experiments). Scale bar, 500 µm. $^*P < 0.05$, $^{**}P < 0.01$, $^{***}P < 0.001$ and $^{****}P < 0.0001$ calculated by chi-square test of independence (**e**, **l**, **q**), two-way repeated measures ANOVA with Bonferroni's post hoc test (**f**–**h**), paired two-tailed *t*-test (**j**), unpaired two-tailed *t*-test (**m**–**o**) and one-way ANOVA with Bonferroni's post hoc test (**r**–**t**). Data are mean ± s.e.m. *P* values are described in the Supplementary Statistical Information.

demonstrate that the COApm has a critical role in the suppression of mating behaviours when male mice are faced with unhealthy females.

Suppression of mating engages the MEA

To gain further insights into the circuit-level mechanisms that underlie COApm suppression of social behaviours, we performed anterograde tracing experiments to identify downstream targets of the COApm. Among the labelled regions, the MEA, which is known to be involved in regulating innate social behaviours[17–20], receives the largest COApm axonal projection (Extended Data Fig. 6a, b). The majority of MEA neurons postsynaptic to the COApm are located in the MEApv, which is enriched for Vglut2$^+$ glutamatergic neurons over Vgat$^+$ GABAergic neurons (Extended Data Fig. 6c–g). We confirmed the functional relevance of the COApm-to-MEA Vglut2$^+$ projection by monitoring the activity of the Vglut2$^+$ or Vgat$^+$ populations in response to optogenetic activation of the COApm. Stimulating the COApm evoked responses preferentially in MEA-Vglut2$^+$ neurons as measured using GCaMP fluorescence (Fig. 3a–e). Moreover, MEA-Vglut2$^+$ neurons, similar to the COApm, were directly activated by LPS females (Extended Data Fig. 6h, i). These data suggest that the COApm suppresses mating behaviour towards LPS females by engaging the MEA-Vglut2$^+$ population. Indeed, optogenetic stimulation of the COApm axonal terminals in the MEA inhibited mating (Fig. 3f) similarly to the stimulation of COApm neuronal cell bodies (Fig. 2a–e). Activation of the MEA-Vglut2$^+$ population also suppressed mating behaviour (Fig. 3g). Conversely, inhibiting the MEA-Vglut2$^+$ population impaired the natural ability of the males to suppress mating towards an unhealthy LPS female (Fig. 3h). Furthermore, using circuit-level functional epistasis experiments, we demonstrated that activation of the COApm axonal terminals, when combined with concurrent inhibition of the MEA-Vglut2$^+$ population, does not suppress mating behaviour (Fig. 3i, also see Extended Data Fig. 7), suggesting that the COApm-to-MEA Vglut2$^+$ projection is required to modulate male mouse mating behaviours on the basis of the perceived health status of the female.

Suppression of mating engages TRH and TRHR

Determining the distinctive transcriptional profile of COApm neurons may provide insight on the genetic basis that enables the COApm to regulate social interactions. To this end, we used viral strategies[21] to label the subset of COApm neurons that specifically project to the MEA-Vglut2$^+$ neurons with a GFP-tagged version of the ribosomal protein L10a (Extended Data Fig. 8a). Following translating ribosome affinity purification (TRAP)[22], we performed RNA sequencing and differential gene-expression analyses, identifying 1,242 differentially expressed genes that are highly enriched in the COApm population that projects to MEA-Vglut2$^+$ neurons (Extended Data Fig. 8b). From these differentially expressed genes, we selected *Trh*—one of the most highly enriched candidates belonging to the neuroactive ligand–receptor interaction pathway—for further analyses (Extended Data Fig. 8c). In situ hybridization confirmed that *Trh* is specifically expressed in the COApm (Fig. 4a, b). Next we functionally tested the role of COApm-TRH$^+$ neurons in suppressing male mating behaviours. Selective activation of TRH$^+$ neurons robustly suppressed mounting towards healthy females (Fig. 4c–h), whereas photostimulation of TRH$^-$ cells did not (Extended

Data Fig. 9a–g), indicating that the ability to modulate mating is restricted to TRH$^+$ neurons in the COApm. Whereas *Trh* is expressed by COApm neurons, *Trhr*—which encodes the TRH receptor TRHR—is selectively enriched in Vglut2$^+$ MEA neurons (Fig. 4i, j), suggesting that TRH may modulate expression of innate social behaviours by acting on the COApm-MEA Vglut2$^+$ circuit. Consistent with this hypothesis, direct delivery of the TRHR agonist taltirelin[23] into the MEA evoked robust responses in Vglut2$^+$ neurons in vitro (Extended Data Fig. 9h–l) and suppressed mating towards healthy females (Fig. 4k–o, Extended Data Fig. 9m). To determine whether TRHR signalling in the MEA is involved in modulating mating behaviours according to the health status of females, we generated a TRHR-conditional-knockout (*Trhr*$^{fl/fl}$) mouse line (Extended Data Fig. 10a). Genetic deletion of TRHR by injection of Cre-expressing virus into the MEA reduced neural activity evoked by photoactivation of COApm-MEA projections (Extended Data Fig. 10b–g) and impaired a male's ability to suppress mating towards LPS females (Fig. 4p–t). These data collectively indicate that suppression of mating behaviour towards an unhealthy mate depends on the COApm-MEA Vglut2$^+$ projection expressing TRH and TRHR.

Discussion

An increasing number of studies suggest that sick individuals engage in a repertoire of sickness behaviours to limit their social interactions[24–27], but little is known about how healthy individuals respond to an infected conspecific. In this study, we have identified an amygdalar circuit responsible for discouraging innate reproductive social behaviours when a male encounters a sick partner. We show that the odour bouquet of a sick female is sufficient to activate the COApm and inhibit male mating behaviours, suggesting that male mice might sense odorants associated with the 'sickness state' of the female mice using odorant receptors such as the formyl peptide family of receptors[12,13]. Posteroventral MEA-Vglut2$^+$ neurons, postsynaptic to the COApm, are essential for the modulation of mating behaviours to unhealthy females. The posterodorsal MEA-Vglut2$^+$ neurons have been previously shown to have a similar role in inhibiting innate social behaviours[17,20], suggesting that Vglut2$^+$ neurons in the dorsal and ventral parts of the posterior MEA could comprise a functional unit partaking in the regulation of social behaviours. Our data also suggest that the COApm-MEA Vglut2$^+$ projection relies on TRH to modulate reproductive social behaviours. Of note, thyroid dysfunction and dysregulated levels of thyroid hormones have been associated with depression and social anxiety in humans[28,29]. Whether TRH has a role in the expression of these symptoms remains to be explored. Overall, our study characterized a novel neural node that takes into account the health status of the interacting partner to modulate innate mating behaviour. As limiting the spread of a pathogen probably requires the concerted efforts of both infected and uninfected individuals, the COApm-MEA Vglut2$^+$ circuit we have identified is likely to contribute to the wellness of an individual as well as its community. It is of paramount importance for an individual to maintain a balance between the drive to socially interact while minimizing risks through social avoidance.

Online content

Any methods, additional references, Nature Research reporting summaries, source data, extended data, supplementary information, acknowledgements, peer review information; details of author contributions and competing interests; and statements of data and code availability are available at https://doi.org/10.1038/s41586-021-03413-6.

1. Tinbergen, N. *The Study of Instinct* (Oxford Univ. Press, 1951).
2. Altizer, S. et al. Social organization and parasite risk in mammals: integrating theory and empirical studies. *Annu. Rev. Ecol. Evol. Syst.* **34**, 517–547 (2003).
3. Hart, B. L. Behavioral adaptations to pathogens and parasites: five strategies. *Neurosci. Biobehav. Rev.* **14**, 273–294 (1990).
4. Ehman, K. D. & Scott, M. E. Female mice mate preferentially with non-parasitized males. *Parasitology* **125**, 461–466 (2002).
5. Chen, P. & Hong, W. Neural circuit mechanisms of social behavior. *Neuron* **98**, 16–30 (2018).
6. Chamero, P. et al. Identification of protein pheromones that promote aggressive behaviour. *Nature* **450**, 899–902 (2007).
7. Hashikawa, K., Hashikawa, Y., Falkner, A. & Lin, D. The neural circuits of mating and fighting in male mice. *Curr. Opin. Neurobiol.* **38**, 27–37 (2016).
8. Stowers, L., Holy, T. E., Meister, M., Dulac, C. & Koentges, G. Loss of sex discrimination and male–male aggression in mice deficient for TRP2. *Science* **295**, 1493–1500 (2002).
9. Leypold, B. G. et al. Altered sexual and social behaviors in trp2 mutant mice. *Proc. Natl Acad. Sci. USA* **99**, 6376–6381 (2002).
10. Medzhitov, R. Toll-like receptors and innate immunity. *Nat. Rev. Immunol.* **1**, 135–145 (2001).
11. Boillat, M. et al. The vomeronasal system mediates sick conspecific avoidance. *Curr. Biol.* **25**, 251–255 (2015).
12. Rivière, S., Challet, L., Fluegge, D., Spehr, M. & Rodriguez, I. Formyl peptide receptor-like proteins are a novel family of vomeronasal chemosensors. *Nature* **459**, 574–577 (2009).
13. Liberles, S. D. et al. Formyl peptide receptors are candidate chemosensory receptors in the vomeronasal organ. *Proc. Natl Acad. Sci. USA* **106**, 9842–9847 (2009).
14. Kavaliers, M., Choleris, E., Agmo, A. & Pfaff, D. W. Olfactory-mediated parasite recognition and avoidance: linking genes to behavior. *Horm. Behav.* **46**, 272–283 (2004).
15. Scalia, F. & Winans, S. S. The differential projections of the olfactory bulb and accessory olfactory bulb in mammals. *J. Comp. Neurol.* **161**, 31–55 (1975).
16. Boehm, U. The vomeronasal system in mice: from the nose to the hypothalamus- and back! *Semin. Cell Dev. Biol.* **17**, 471–479 (2006).
17. Choi, G. B. et al. Lhx6 delineates a pathway mediating innate reproductive behaviors from the amygdala to the hypothalamus. *Neuron* **46**, 647–660 (2005).
18. Li, Y. et al. Neuronal representation of social information in the medial amygdala of awake behaving mice. *Cell* **171**, 1176–1190 (2017).
19. Ishii, K. K. et al. A labeled-line neural circuit for pheromone-mediated sexual behaviors in mice. *Neuron* **95**, 123–137 (2017).
20. Hong, W., Kim, D. W. & Anderson, D. J. Antagonistic control of social versus repetitive self-grooming behaviors by separable amygdala neuronal subsets. *Cell* **158**, 1348–1361 (2014).
21. Wickersham, I. R., Finke, S., Conzelmann, K. K. & Callaway, E. M. Retrograde neuronal tracing with a deletion-mutant rabies virus. *Nat. Methods* **4**, 47–49 (2007).
22. Heiman, M. et al. A translational profiling approach for the molecular characterization of CNS cell types. *Cell* **135**, 738–748 (2008).
23. Suzuki, M., Sugano, H., Matsumoto, K., Yamamura, M. & Ishida, R. Synthesis and central nervous system actions of thyrotropin-releasing hormone analogues containing a dihydroorotic acid moiety. *J. Med. Chem.* **33**, 2130–2137 (1990).
24. Hart, B. L. Biological basis of the behavior of sick animals. *Neurosci. Biobehav. Rev.* **12**, 123–137 (1988).
25. Lopes, P. C., Block, P. & König, B. Infection-induced behavioural changes reduce connectivity and the potential for disease spread in wild mice contact networks. *Sci. Rep.* **6**, 31790 (2016).
26. Van Kerckhove, K., Hens, N., Edmunds, W. J. & Eames, K. T. The impact of illness on social networks: implications for transmission and control of influenza. *Am. J. Epidemiol.* **178**, 1655–1662 (2013).
27. Stockmaier, S., Bolnick, D. I., Page, R. A. & Carter, G. G. Sickness effects on social interactions depend on the type of behaviour and relationship. *J. Anim. Ecol.* **89**, 1387–1394 (2020).
28. Fischer, S. & Ehlert, U. Hypothalamic-pituitary-thyroid (HPT) axis functioning in anxiety disorders. A systematic review. *Depress. Anxiety* **35**, 98–110 (2018).
29. Baumgartner, A. Thyroxine and the treatment of affective disorders: an overview of the results of basic and clinical research. *Int. J. Neuropsychopharmacol.* **3**, 149–165 (2000).

Methods

Mice

All experiments were performed according to the Guide for the Care and Use of Laboratory Animals and were approved by the National Institutes of Health and the Committee on Animal Care at Massachusetts Institute of Technology. C57BL/6J (000664), Slc32a1(Vgat)-Cre (028862), Slc17a6(Vglut2)-Cre (016963), and Ai14 (007914) mice were purchased from Jackson Laboratories and inbred. Generation of Trh-IRES-Cre mice has been described[30]. To develop a conditional-knockout mouse line that removes *Trhr* in a Cre-dependent manner, a targeting vector with two *loxP* sites flanking common exons 1 and 2 was generated using the CRISPR–Cas9 system (Biocytogen). For PCR genotyping, the following primers were used: EGE-WFZ-023-5′loxp-F 5′-GTTCTGATGCCCAGATGGTCCTGTC-3′, EGE-WFZ-023-5′loxp-R 5′-TG CAGTCCCCAGGGCTTGAGATAAA-3′ for WT 301bps/Floxed 378 bp and EGE-WFZ-023-3′loxP-F 5′-ACTGAGTGTGCTTTTAGAACCATGT-3′, EGE-WFZ-023-3′loxP-R 5′- TTTGGTTAATGGCCAGCTACACCTT-3′ for WT 342 bp/Floxed 415 bp. Mice were housed at 20–22 °C, 40–60% humidity and a 12-h light cycle and given ad libitum access to food and water. All mice were males aged 2–5 months unless otherwise specified.

Stereotaxic surgery

Surgeries were carried out using aseptic techniques. Mice were anaesthetized using a mixture of ketamine (100 mg kg^{-1}, intraperitoneal injection) and xylazine (10 mg kg^{-1}, intraperitoneal injection). Mice were given preoperative slow-release buprenorphine (1.0 mg kg^{-1}, subcutaneous injection). Injection coordinates from bregma in mm: COApm, ±2.9 ML, −2.9 AP, −5.7 DV; MEApv, ±2.1 ML, −1.7 AP, −5.6 DV; MEApd, ±2.2 ML, −1.7 AP, −5.4 DV; AOB, +1.0 ML, +4.25 AP, −1.8 DV with a 20° angle relative to AP. Injections were performed using a pulled fine-glass capillary at 0.1 µl min^{-1}, 1 µl total for Cre-dependent viruses and 0.4 µl otherwise. For fibre photometry, AAV_1-Syn-GCaMP6s or AAV_1-Syn-FLEX-GCaMP7f (Penn Vector Core)[31] were delivered to COApm of wild-type mice or MEA of Vglut2-Cre mice, respectively, in the right hemisphere with a 400-µm diameter optic fibre implanted 300 µm above the injection targets. For experiments involving optical stimulation[32], wild-type or Vgat/Vglut2/Trh-Cre mice received bilateral stereotaxic injections of AAV_2-hSyn-hChR2-eYFP (UNC Vector Core) or AAV_2-Ef1α-DIO-hChR2-eYFP (UNC Vector Core), respectively, with 300-µm optic fibres implanted 200 µm above the injection targets. Control groups were injected with AAV_2-hSyn-eYFP or AAV_2-Ef1α-DIO-eYFP, respectively, with optic fibres implanted similarly. For photoactivation of COApm-MEA projections, wild-type mice received bilateral injections of virus (AAV_2-hSyn-hChR2-eYFP) to COApm with optic fibres implanted in MEA. For MEA fibre photometry with COApm photoactivation, Vgat/Vglut2-Cre mice received unilateral injections of virus encoding ChrimsonR (AAV_2-hSyn-ChrimsonR-tdTomato (UNC)) to COApm and virus encoding GCaMP6s (AAV_1-CAG-Flex- GCaMP6s) to MEA. A 300-µm optic fibre was implanted in COApm for photoactivation and a 400-µm optic fibre was implanted in MEA for fibre photometry. Optic fibres were prepared in-house as described previously[33]. For photoactivation of AOB, wild-type mice received unilateral injection of AAV_2-hSyn-hChR2-eYFP to AOB. For photoactivation of TRH^- cells, Trh-Cre mice received unilateral injection of $AAV_{1/2}$-Ef1a-DO-hChR2-mCherry (Addgene 370820) to COApm. Control group was injected with $AAV_{1/2}$-Ef1a-DO-DIO-TdTomato-eGFP (Addgene 37120). For DREADD inhibition experiments[34], wild-type or Vglut2-Cre mice received bilateral stereotaxic injections of AAV_2-hSyn-hM4D(G_i)-mCherry (Addgene) or AAV_2-hSyn-DIO-hM4D(G_i)-mCherry (Addgene), respectively, in either COApm or MEA. AAV_2-hSyn-mCherry or AAV_2-hSyn-DIO-mCherry were used for control groups, respectively. For administration of taltirelin into MEA, guide cannulas (26 gauge, PlasticsOne) were implanted 500 µm above the MEA (±2.2 ML, −1.7 AP, −5.1 DV). Guide cannulas were fitted with dummy cannulas to maintain cannula patency after surgery. For genetic removal of *Trhr* in the MEA, wild-type or homozygous *Trhr* conditional-knockout mice ($Trhr^{fl/fl}$) received bilateral injection of AAV_1-hSyn-GFP or AAV_1-Syn-Cre in the MEA. Removal of the vomeronasal organ was performed as previously described[35]. In brief, mice were anaesthetized and the lower jaw was gently opened and fixed with a home-made mouth holder. A midline incision was made in the soft palate and the underlying bone was exposed. The rostral end of the vomeronasal organ (VNO) was exposed and bilaterally removed. The resulting cavity was filled with a gel foam and the incision was closed with absorbable sutures. All mice recovered for at least one week before behavioural testing.

Virus preparation

Chimeric AAV_1/AAV_2[36] viruses were prepared with plasmids for pAAV-Ef1a-DO-hChR2-mCherry (Addgene 370820) and pAAV-Ef1a-DO-DIO-TdTomato-eGFP (Addgene 37120). In brief, AAV plasmids, AAV_1/AAV_2 Rep/Cap, and adenovirus-helper plasmid (pFdelta6) were transfected into HEK293FT cells and incubated for 3 days. Cells were lysed and rAAVs collected by centrifugation to remove cellular debris. Finally, rAAVs were purified using heparin columns.

Tissue-slice preparation and immunohistochemistry

Mice were transcardially perfused with cold paraformaldehyde (PFA) (4% in PBS). Brains were kept in PFA overnight at 4 °C before vibratome sectioning (Leica VT1000s). Brains were cut at 50-µm thickness for FOS immunohistochemistry. Brains were cut at 100-µm thickness for all other experiments. Sections were incubated in blocking solution (0.4% Triton X-100 and 2% goat serum in PBS) for 30 min. Sections were then incubated in blocking solution containing rabbit anti-FOS (1:500, Millipore, ABE457) primary antibody overnight at room temperature. Sections were washed in wash buffer (0.4% Triton X-100 in PBS) three times and incubated in blocking solution containing Alexa 488 Goat anti-rabbit (1:250, Life Technologies, A11034) secondary antibodies and DAPI (1:5,000, D1306, Thermo Fisher) for 2 h at room temperature. Images of stained slices were acquired using confocal microscopes (LSM710 and LSM900, Carl Zeiss) with a 10×, 20× or 40× objective lens.

Anatomical tracing

For anterograde tracing of COApm axonal projections, wild-type mice received unilateral stereotaxic injections of virus (AAV_2-hSyn-tdTomato) into COApm. 4 weeks later, mice were euthanized and 100-µm-thick coronal brain slices were prepared. Images were taken at 300-µm intervals from brain regions expressing tdTomato using a confocal microscope (LSM710, Carl Zeiss). Using Zen software (Carl Zeiss), regions of interest were defined based on the Paxinos brain atlas[37] and total fluorescence intensity in each region was calculated. For anterograde trans-synaptic tracing, AAV_1-hSyn-Cre (0.5µl) virus was injected into AOB in Ai14 reporter mice that express tdTomato in a Cre-dependent manner. After two weeks, mice were euthanized and coronal brain sections were prepared of BST (AP: 0.2 to −0.4), MEA (AP: −1.2 to −2.1) and COApm (−2.4 to −3.2). Images were taken every 200 µm using a confocal microscope (LSM710, Carl Zeiss) and the number of tdTomato-positive cells were manually counted. For anterograde trans-synaptic tracing of COApm, the same histological and imaging procedures were used for MEA (AP −1.7).

Quantification of FOS^+ cells

For FOS expression studies after interaction with healthy or sick females, subject male mice were co-housed with a female for 3 days for habituation. The female was separated and intraperitoneally injected with either PBS or LPS and returned to the male cage 2 h later. Males were euthanized 90 min after a 2-min free interaction with the female and brains were processed for immunohistochemical detection of FOS protein. All cells were counted bilaterally from two coronal sections of each respective brain region, as defined by the Paxinos brain atlas[37].

Regions quantified include: AOBmi, AOBgr, BST, MEApd, MEApv and COApm. For FOS expression studies after interaction with PBS or LPS odour, males were euthanized 90 min after a 2-min exposure to urine and faeces obtained from females intraperitoneally injected with PBS (PBS odour) or LPS (LPS odour) and brains were processed for immunohistochemical detection of FOS protein in the COApm. For FOS expression studies after photoactivation, males were euthanized 90 min after photoactivation of AOB or COApm and brains were processed for immunohistochemical detection of FOS protein in the COApm.

Fibre photometry

The fibre photometry system was built as previously described[38]. In brief, blue light from a 473 nm diode laser (LRS473, Laserglow) was chopped at 197 Hz and reflected off of a dichroic mirror (FF495, Semrock) and coupled into a 600-µm optical fibre patch cord (0.48NA, Thorlabs, BFH48-600) through a microscope objective (40× 0.65 NA, Olympus). The patch cord was coupled with a free optic fibre, which has the same light efficiency as the implanted one, and light power at the fibre tip was set to 20 µW. The patch cord was connected to an implanted 400-µm optical fibre via a ceramic sleeve. GCaMP6s fluorescence was collected through a bandpass filter (FF01-520/35) into a photodetector (2151, NewFocus). The signal was passed through a lock-in amplifier (Model SR810, Stanford Research Systems) and digitized and collected with a LabVIEW DAQ (100Hz sampling frequency, LabVIEW), and recorded with custom LabVIEW software. Mouse behaviour was recorded using EthoVision XT tracking system (Noldus) and time-stamped with photometry data using the LabVIEW TTL pulse. Male mice expressing GCaMP in COApm or MEA were single housed and habituated with fibre coupling in their home cage placed in the behaviour chamber for 30 min. During this habituation, the fluorescence signal level was checked and the mice showing basal fluorescence level between 3 to 5 amplitudes were used for further experiments to minimize the signal intensity variation between mice, which might be caused by variable GCaMP expression levels and optic fibre placements. A stimulus mouse (PBS or LPS females in oestrus; oestrus or dioestrus healthy females; healthy females painted with PBS or LPS odour) or stimulus odour (PBS or LPS odour) were presented for 10 min in sequential and counterbalanced sessions with an 1-h interval in between the sessions. Urine and faeces from PBS- or LPS-treated females served as PBS or LPS odour, respectively. The raw fluorescence signal was normalized to the mean of the 1-min baseline before the first contact for *z*-score calculation. The mean *z*-score of fluorescence during direct investigation was calculated from the first 3-min periods. For the generation of the heat map, *z*-scored fluorescence signals were further normalized to minimum and maximum values.

Behavioural analyses

All behaviour experiments were performed between 3 h before and after light offset time (light offset: 19:00). Mice were transferred to the testing area at least three hours before the initiation of experiments. Tracking of mouse behaviour was done using the EthoVision XT (Noldus) tracking system.

Mating assays. Naive C57BL/6J females were used. All females were in oestrus, unless otherwise indicated to be in dioestrus. Oestrus phase was checked by vaginal smear on the testing day[39]. Male mice were first screened for mounting behaviour. After 30 min of habituation, they were presented with a female in the males' home cage for 5 min. Only the males that mounted the female within the first 5-min period were used for experimentation. Males that successfully mounted were then single-housed for a minimum of three days before the behaviour test. For testing, the home-cage of a male mouse was placed in a behavioural chamber with recording capabilities with a side view camera. After a 10-min acclimatization in the behavioural chamber, an intruder female was placed into the male's home cage for 10 min before being removed. For the experiments described in Extended Data Fig. 1a–c only, two females were simultaneously introduced. Intruder females were either untreated, or intraperitoneally injected with PBS (PBS female) or LPS (LPS female, 0.5 mg kg^{-1}) 2 h before testing, or painted with urine and faeces from PBS-females (PBS odour) or LPS females (LPS odour). Male mounting attempts (percentage of males engaged in mounting, mounting time, number of mounts, and latency to the first mounting attempt), investigation (sniffing of facial or anogenital regions), and social or self-grooming were manually scored. Four different categories of female behaviours (run, the display of an active escaping behaviour from males' mounting attempts; rear up, the display of a defensive posture by facing up against the male during mounting attempts; sit, the display of a passive, non-receptive response by sitting down and not exposing the genital region during males' mounting attempts; lordosis, the display of receptive responses, including the canonical lordosis posture with the curved spine and a standing posture with four limbs without the curved spine, that allow for males mounting) displayed upon males' mounting attempts were manually scored. For the behavioural raster plots shown in Extended Data Fig. 1i, female behaviours during the rest of the interactions were also analysed and these include exploration of the cage, which is a novel environment to the females (for example, sniffing and digging), and a sitting posture. The presence of mating plugs in females was determined 24 h following the mating assay to oestrus versus dioestrus females, in which the females stayed with the males after the 10-min test.

Mating assays with optogenetic activation. ChR2, eYFP or td Tomato was virally targeted to COApm, COApm-TRH^+, COApm-TRH^- or MEA-$Vglut2^+$ neurons and optic fibres were bilaterally implanted. Mice were habituated for fibre coupling a day before testing. On the testing day, an optic cable was connected to the optic fibre to deliver 405 nm laser stimulation. After a 10-min acclimatization, a female was placed in the subject's home cage. Mice behaviour was monitored through a side-view camera and a 10-s photoactivation (2 mW, 20-Hz square wave, 10-ms pulse width) was manually triggered at each instance of contact investigation.

Mating assays with DREADD inhibition. Male mice expressing hM4Di or mCherry in COApm or MEA-$Vglut2^+$ neurons were habituated for intraperitoneal injection a day before testing in the testing room. On the testing day, clozapine *N*-oxide (1 mg kg^{-1}) was diluted in sterile saline and intraperitoneally administered to male mice 40 min before testing.

Mating assays with concurrent photoactivation of COApm-MEA projections and DREADD inhibition of MEA-$Vglut2^+$ neurons. Experimental group mice were Vglut2-Cre male mice bilaterally expressing ChR2 in COApm and hM4Di in MEA-$Vglut2^+$ neurons with optic fibres implanted in MEA. Control group mice were Vglut2-Cre mice expressing ChR2 in COApm and mCherry in MEA-$Vglut2^+$ neurons. Clozapine *N*-oxide (1 mg kg^{-1}) was diluted in sterile saline and administered to male mice 40 min before testing. Photoactivation of COApm-MEA projections was manually triggered at each instance of contact investigation.

Mating assays with taltirelin injection to MEA. Wild-type male mice with guide cannulas implanted in MEA were habituated for injection cannula insertion a day before testing. On the testing day, mice were briefly anaesthetized using isoflurane, and either vehicle or taltirelin (10 ng per side in 0.5 µl at a rate of 180 nl min^{-1}, 7956-ML/CF, R&D) was administered bilaterally into the MEA through 500-µm projecting injector tips (PlasticsOne). Mice were returned to the home cage and placed in a behavioural chamber. Twenty minutes after administration of vehicle or taltirelin, mice were assayed for mating behaviour. Cannula placements were histologically verified.

Feeding assay. Male mice expressing ChR2 in COApm were single-housed and food-deprived for 12 h. Mice were then connected to optic fibres and placed back in their home cage. After 10 min, a single pre-weighed food pellet was placed in the centre of their home cage. The amount of time spent eating was measured over a ten-minute period, and the pellet was removed and re-weighed to calculate the amount of food eaten. Photoactivation of COApm (2 mW, 20-Hz square wave, 20% duty cycle) occurred throughout the 10-min testing period.

Three-chamber social-approach assay. Single-housed male mice expressing ChR2 in COApm were assayed for sociability using a three-chamber social-approach assay. The arena was constructed of white acrylic (50 cm × 35 cm × 30 cm). Wire cups (Spectrum Diversified) were placed in the back left and right corner of the arena beneath water-filled 1-l bottles (Nalgene). On day 0, mice were habituated to the arena for 20 min and returned to their home cage. On day 1, mice were connected to optic fibres and placed in the centre of the arena and allowed to freely explore. Following 10 min of habituation, mice were confined to the centre of the arena. An inanimate object (rubber stopper) or a male conspecific were placed beneath the wire cups. Placement of the inanimate object and social target were alternated. Mice were then allowed to freely explore the arena for 10 min. During this period, photoactivation of COApm (2 mW, 20-Hz square wave, 20% duty cycle) was automatically triggered during interaction with either the inanimate object or social target. Interaction time was defined as time spent in the areas circumscribing the wire cups (<2 cm). Sociability was defined as interaction time with the social target divided by total interaction time and expressed as a percentage.

Three-chamber social-preference assay. Single-housed wild-type mice were used for the behavioural assay as described in 'Three-chamber social-approach assay', except the target objects were PBS- and LPS-treated females.

Real-time place preference. Male mice expressing ChR2 in COApm were assayed for preference of COApm photoactivation in a RTPP assay. The arena consisted of two chambers constructed of white acrylic (30 cm × 30 cm). Mice were connected to optic fibres and placed in the left chamber. Photoactivation of COApm (2 mW, 20-Hz square wave, 20% duty cycle) was triggered whenever the mouse entered the right chamber. Stimulation preference was defined as the time spent in the chamber paired with photoactivation divided by total trial duration (10 min) and displayed as a percentage.

In situ hybridization

Fluorescence in situ hybridization (FISH) was conducted with ACDBio RNAscope Multiplex Fluorescence Assay. The following probes were used: C1: Trhr (Mm-Trhr: 443771), C2: Vglut2 (Mm-Slc17a6-C2: 319171-C2), C3: Vgat (Mm-Slc32a1-C3: 319191-C3); C1: Trh (Mm-Trh: 436811). Brain tissues were obtained from age-matched 8- to 10-week-old sexually naive male C57BL/6J mice and immediately fresh-frozen in optimal cutting temperature (OCT) medium on dry ice. Twenty-micrometer sections were obtained using a cryostat (Leica, Germany) and stored at − 80 °C. RNAscope procedures were performed according to the user manual provided by ACDBio with modifications specified as following. In brief, sections were fixed with 4% chilled paraformaldehyde (PFA) for 15 min and washed in 1× phosphate-buffered saline (PBS) twice for 2 min each. Sections were then dehydrated consecutively in 50%, 75%, 100% and 100% ethanol for 5 min each. Tissue was digested with Protease IV for 13 min at room temperature and washed twice in 1× PBS with agitation. Vglut2 and Vgat probes were diluted 1: 50 in *Trhr* probe solution and pipetted onto each slide. Probe hybridization was conducted for 2 h and 30 min at 40 °C and slides were then washed in 1× wash buffer twice for 4 min each. Sections were then incubated at 40 °C in Amp1 for 35 min, Amp2 for 17 min, Amp3 for 35 min and Amp4 for 17 min, with two 1× wash buffer rinses between each incubation. Sections were finally treated with DAPI for 30 s, mounted with CC/Mount and stored at 4 °C. Images were acquired using Zeiss LSM 710 and LSM900 confocal microscopes (40× objective, 1.2 NA) and a Zeiss Axio Imager.Z2 microscope (10× objective, 0.45 NA). Imaging settings were established during the first acquisition and not modified afterwards. Target genes (*Trh*, *Trhr*, *Vgat* and *Vlut2*) and DAPI expression were quantified using QuPath[40]. For *Trh* quantification, cells were divided into the following categories based on level of *Trh* expression: low, 1–3 puncta; medium, 4–9 puncta; high, 10–15 puncta; highest, >15 puncta. For co-expression of *Vglut2*, *Vgat* and *Trhr*, cells were classified as positive if the level of target expression was >3 puncta. Percentage of co-expression is calculated as the number of *Vglut2* and *Trhr* or *Vgat* and *Trhr* double-positive cells divided by the total number of *Trhr*-positive cells. For validation of conditional knockout of *Trhr* in the MEA, *Trhr* probe was used on brain tissues from $Trhr^{fl/fl}$ mice, which received stereotaxic injections of AAV_1-Syn-Cre in MEApv. $Trhr^{fl/fl}$ mice without virus injection served as a control. To quantify the percentage of MEApv neurons expressing *Trhr*, cells were classified as Trhr-positive if the level of target expression was >1 puncta.

Calcium imaging of MEA brain slices

Slice preparation. Virus (AAV_1-Syn-FLEX-GCaMP7f) was bilaterally delivered to MEA of vGlut2-Cre mice. Four to eight weeks after the virus injection, mice were anaesthetized with isoflurane. Before decapitation, intracardiac perfusion was performed with an ice-cold cutting solution containing (in mM): 96 *N*-methyl-D-glucamine (NMDG), 2.5 KCl, 10 $MgSO_4$, 0.5 $CaCl_2$, 1.25 NaH_2PO_4, 25 $NaHCO_3$, 25 glucose, 17.5 HEPES, 5 sodium ascorbate, 2 thiourea, 3 sodium pyruvate, 12 L-acetyl-cysteine, perfused with 95% O_2 and 5% CO_2 (pH 7.3–7.4 adjusted by HCl after bubbling). Coronal slices of the MEA (300 µm thick) were obtained by a vibratome (VT1200s, Leica) in the ice-cold cutting solution. The slices were immediately transferred to the same cutting solution at 34 °C for 10 min, and then transferred to slice holding solution at room temperature containing (in mM): 94 NaCl, 2.5 KCl, 2 $MgSO_4$, 2 $CaCl_2$, 1.25 NaH_2PO_4, 25 $NaHCO_3$, 25 glucose, 14 HEPES, 5 sodium ascorbate, 2 thiourea, 3 sodium pyruvate, 12.3 L-acetyl-cysteine, perfused with 95% O_2 and 5% CO_2 (pH 7.3–7.4 adjusted by NaOH after bubbling). The slices were recovered in the holding solution for a minimum of 1.5 h. All experiments were done within 6 h from the start of the recovery.

Image acquisition and data analysis. Slices were transferred from the holding solution to an immersion recording chamber perfused with artificial cerebrospinal fluid (ACSF) containing (in mM): 126 NaCl, 4 KCl, 1 $MgCl_2$, 1 $CaCl_2$, 1 NaH_2PO_4, 26 $NaHCO_3$, 20 glucose, perfused with 95% O_2 and 5% CO_2. Flow of ACSF into the recording chamber was at a rate of 3 ml min^{-1} and its temperature was maintained at 33–34 °C by a temperature controller (TC-324C, Warner Instruments). An upright microscope (SliceScope Pro 2000, Scientifica) with a 40× water-immersion objective lens (LUMPLFLN40XW, Olympus), 490-nm LED illumination (pE-100, CoolLED) and a GFP filter set (49002, Chroma). Images were acquired at 10 Hz (2 × 2 digital binning, 1,024 × 1,024-pixel resolution) with an sCMOS camera (Prime BSI, Teledyne Photometrics) using Micro-manager open-source software for 30 s before and 150 s after taltirelin application. EZcalcium open-source MATLAB toolbox[41] was used for motion correction and automated ROI (region of interest) detection. Round-shaped, soma-like ROIs were manually selected for extracting neuronal fluorescence signals. Fluorescence signal of each MEA slice was obtained by averaging changes in fluorescence ($\Delta F/F$) of individual neurons ($n = 336$ cells from 6 slices). The fluorescence signal of individual MEA slices were used to obtain the average fluorescence trace shown in Extended Data Fig. 9k.

In vivo recording of MEA responses upon photoactivation of COApm inputs

MEA responses to COApm inputs in *Trhr* conditional-knockout mice were tested by recording local field potentials (LFPs) in anaesthetized

mice. *Trhr*$^{fl/fl}$ mice were unilaterally injected with AAV_2-hSyn-ChR2-eYFP in COApm and AAV_1-hSyn-GFP or AAV_1-hSyn-Cre in the ipsilateral MEApv. Four weeks after the viral injections, mice were anaesthetized using a mixture of ketamine (100 mg kg^{-1}, intraperitoneal injection) and xylazine (10 mg kg^{-1}, intraperitoneal injection) and placed in a stereotaxic frame. A homemade optrode, which consists of an optic fibre (200 µm) and two-channel tungsten electrodes (5 MΩ, 300-µm projection from the optic fibre tip), were lowered to MEApv. LFPs were recorded starting at DV = -5.0 mm from the bregma, while the electrode was being lowered, to find the locus of the maximum response evoked by a single pulse of photoactivation (405-nm laser, 2 mW, 10 ms) of COApm inputs. Recordings were amplified, band-pass filtered between 10 and 300 Hz and digitized at 10 kHz using a Digital Lynx 4SX system (Neuralynx). TTL event signals for photoactivation from a pulse generator were aligned to the recorded waveforms using the Neuralynx system. Light-evoked local field potentials were analysed off-line using a (ADInstrument, NeuroExplorer5). Three waveforms evoked by photostimulations delivered at 1-min intervals were averaged to obtain the baseline-to-negative peak amplitude for individual mice.

RNA sequencing

Labelling of COApm cells projecting to MEA. Vglut2-Cre mice received stereotaxic injections of a virus mixture (AAV_1-Syn-FLEX-TTA and AAV_1-TRE-B19G, total 0.5 µl)[42] into MEApv (±2.1 ML, −1.7 AP, −5.6 DV). After 2 weeks, glycoprotein gene deleted rabies virus (RVΔG-4eGFP-L10a (EnvA)) was targeted to the same coordinates. Five days later, COApm tissues were collected and immediately used for TRAP purifications as described below. For the control group, 100 µl of AAV.PHP.eB-Syn-L10a-eGFP (1.13×10^{11} VG per mouse; SignaGen Laboratories) was retro-orbitally injected. COApm tissue was collected at 3 weeks post-injection and used immediately for TRAP purifications.

TRAP purifications. Brain-tissue dissections were performed on ice after cooling the head in liquid nitrogen for 4 s. After dissection, cell-type-specific mRNAs were purified according to the established TRAP protocol[43]. COApm tissue was homogenized with a glass/Teflon power-driven Potter–Elvehjem homogenizer in an ice-cold lysis buffer (150 mM KCl, 10 mM HEPES pH 7.4, 5 mM $MgCl_2$, 0.5 mM dithiothreitol, 100 µg ml^{-1} cycloheximide, 20 U µl^{-1} SUPERaseIn RNase Inhibitor, 40 U µl^{-1} RNasin Plus Rnase Inhibitor, and EDTA-free protease inhibitors). Following homogenization, samples were centrifuged at 2,000*g* at 4 °C for 10 min and the supernatant was transferred to a new tube. NP-40 (final concentration 1%) and 1,2-diheptanoyl-*sn*-glycero-3-phosphocholine (final concentration 15 mM) were subsequently added and samples were incubated on ice for 5 min. Samples were centrifuged at 13,000*g* at 4 °C for 10 min and the supernatant was transferred to a new tube. Streptavidin Dynabeads (ThermoFisher Scientific) coated with biotin-linked mouse anti-GFP antibodies were then added to this supernatant and the samples were incubated overnight at 4 °C with end-over-end rotation. Beads were collected on a magnetic rack and washed three times with wash buffer (350 mM KCl, 10 mM HEPES pH 7.4, 5 mM $MgCl_2$, 0.5 mM dithiothreitol, 100 µg ml^{-1} cycloheximide, 1% NP-40). RNA was subsequently purified using the Absolutely RNA Isolation Nanoprep kit (Agilent Technologies). To ensure quality and accurate quantitation, purified RNA was run on a Bioanalyzer using the RNA 6000 Pico Kit (Agilent Technologies).

TRAP RNA sequencing and analysis. Purified TRAP samples were prepared for RNA-Seq using the Takara Bio Smart-Seq v4 kit (Takara Bio). RNA-Seq was performed on an Illumina HiSeq 4000 at the University of California, San Francisco Functional Genomics Core. FASTQ files were aligned to the *Mus musculus* genome build GRCm38 and annotation build 96 (reference FASTA and GTF file) using STAR v2.7.2b. Read counts were generated by STAR using the–quantMode GeneCounts option, using the default options. Only mapped reads uniquely assigned to the mouse genome were used for differential expression testing. These were imported into R and then converted to normalized read counts with DESeq2[44]. Differential Expression was performed using DESeq2, and significant genes were filtered by a *q* value (false discovery rate) threshold of 1×10^{-15}. To remove systemic bias possible from the use of rabies virus[45,46], genes involved in the following MSigDB hallmark gene sets were further removed: interferon gamma response, interferon alpha response, allograft rejection, IL-6 JAK STAT3 signalling, TNF signalling via NF-κB, inflammatory response, complement, G2M checkpoint, E2F targets, and IL-2 STAT5 signalling. These differentially expressed genes were then compared to the set of COApm-enriched genes (relative to the grey matter) obtained from Allen Brain Atlas Differential Search with the expression threshold set to 1. For KEGG pathway analysis, differentially expressed genes were processed using Enrichr[47,48].

Statistics and reproducibility

Statistical analyses were performed using GraphPad Prism. Sample sizes were chosen on the basis of similar previous studies[20,49], and not on statistical methods to predetermine sample sizes. Within each iteration of an experiment, mice were randomly assigned to groups with approximately balanced sample sizes. Behavioural results from mice with inaccurate targeting of viral infection or cannula implantations were excluded.

Reporting summary

Further information on research design is available in the Nature Research Reporting Summary linked to this paper.

Data availability

Source data are provided in the Supplementary Information. Sequencing data sets are publicly available in NCBI Gene Expression Omnibus (GEO) under accession GSE167176. All data are available from the corresponding author upon request.

30. Krashes, M. J. et al. An excitatory paraventricular nucleus to AgRP neuron circuit that drives hunger. *Nature* **507**, 238–242 (2014).
31. Chen, T. W. et al. Ultrasensitive fluorescent proteins for imaging neuronal activity. *Nature* **499**, 295–300 (2013).
32. Zhang, F. et al. Optogenetic interrogation of neural circuits: technology for probing mammalian brain structures. *Nat. Protoc.* **5**, 439–456 (2010).
33. Ung, K. & Arenkiel, B. R. Fiber-optic implantation for chronic optogenetic stimulation of brain tissue. *J. Vis. Exp.* **68**, e50004 (2012).
34. Armbruster, B. N., Li, X., Pausch, M. H., Herlitze, S. & Roth, B. L. Evolving the lock to fit the key to create a family of G protein-coupled receptors potently activated by an inert ligand. *Proc. Natl Acad. Sci. USA* **104**, 5163–5168 (2007).
35. Pankevich, D. E., Baum, M. J. & Cherry, J. A. Olfactory sex discrimination persists, whereas the preference for urinary odorants from estrous females disappears in male mice after vomeronasal organ removal. *J. Neurosci.* **24**, 9451–9457 (2004).
36. McClure, C., Cole, K. L., Wulff, P., Klugmann, M. & Murray, A. J. Production and titering of recombinant adeno-associated viral vectors. *J. Vis. Exp.* **57**, e3348 (2011).
37. Paxinos, G. & Franklin, K. B. J. *The Mouse Brain in Stereotaxic Coordinates* 2nd edn (Elsevier/Academic Press, 2004).
38. Gunaydin, L. A. et al. Natural neural projection dynamics underlying social behavior. *Cell* **157**, 1535–1551 (2014).
39. Byers, S. L., Wiles, M. V., Dunn, S. L. & Taft, R. A. Mouse estrous cycle identification tool and images. *PLoS ONE* **7**, e35538 (2012).
40. Bankhead, P. et al. QuPath: Open source software for digital pathology image analysis. *Sci. Rep.* **7**, 16878 (2017).
41. Cantu, D. A. et al. EZcalcium: open-source toolbox for analysis of calcium imaging data. *Front. Neural Circuits* **14**, 25 (2020).
42. Chan, K. Y. et al. Engineered AAVs for efficient noninvasive gene delivery to the central and peripheral nervous systems. *Nat. Neurosci.* **20**, 1172–1179 (2017).
43. Heiman, M., Kulicke, R., Fenster, R. J., Greengard, P. & Heintz, N. Cell type-specific mRNA purification by translating ribosome affinity purification (TRAP). *Nat. Protoc.* **9**, 1282–1291 (2014).
44. Love, M. I., Huber, W. & Anders, S. Moderated estimation of fold change and dispersion for RNA-seq data with DESeq2. *Genome Biol.* **15**, 550 (2014). 8
45. Hornung, V. et al. 5′-Triphosphate RNA is the ligand for RIG-I. *Science* **314**, 994–997 (2006).
46. Huang, K. W. & Sabatini, B. L. Single-cell analysis of neuroinflammatory responses following intracranial injection of G-deleted rabies viruses. *Front. Cell. Neurosci.* **14**, 65 (2020).

47. Chen, E. Y. et al. Enrichr: interactive and collaborative HTML5 gene list enrichment analysis tool. *BMC Bioinformatics* **14**, 128 (2013).
48. Kuleshov, M. V. et al. Enrichr: a comprehensive gene set enrichment analysis web server 2016 update. *Nucleic Acids Res.* **44** (W1), W90–W97 (2016).
49. Choe, H. K. et al. Oxytocin mediates entrainment of sensory stimuli to social cues of opposing valence. *Neuron* **87**, 152–163 (2015).

Acknowledgements We thank N. Soares, M. Andina, K. Ronayne and I. D. Mejia for assistance with experiments; B. Noro and M. Trombly for critical reading of the manuscript; J. Huh for his contribution to the conceptual development of the project; B. Lowell for generously sharing the *Trh*-Cre mouse line; and H. Choi for the fibre photometry setup. This work was supported by the National Institute of Mental Health grants R01 MH122270 and R01 MH106497 (G.B.C.), the JPB Foundation (M.H. and G.B.C), Simons Center for the Social Brain Postdoctoral Fellowship (J.-T.K. and H.K.C.) and the Picower Fellows (J.-T.K. and H.L.).

Author contributions J.-T.K. and G.B.C. conceptualized the study. J.-T.K., H.L., C.R., M.H. and G.B.C. designed the experiments and/or provided advice and technical expertise. J.-T.K., H.L., C.R., A.S., J.F., D.H.C., S.B., H.A.S. and H.K.C. performed the experiments. I.R.W. provided reagents. J.-T.K. and G.B.C. wrote the manuscript with inputs from the co-authors.

Competing interests The authors declare no competing interests.

Additional information
Supplementary information The online version contains supplementary material available at https://doi.org/10.1038/s41586-021-03413-6.
Correspondence and requests for materials should be addressed to G.B.C.
Peer review information *Nature* thanks Dayu Lin, Ruslan Medzhitov and the other, anonymous, reviewer(s) for their contribution to the peer review of this work.

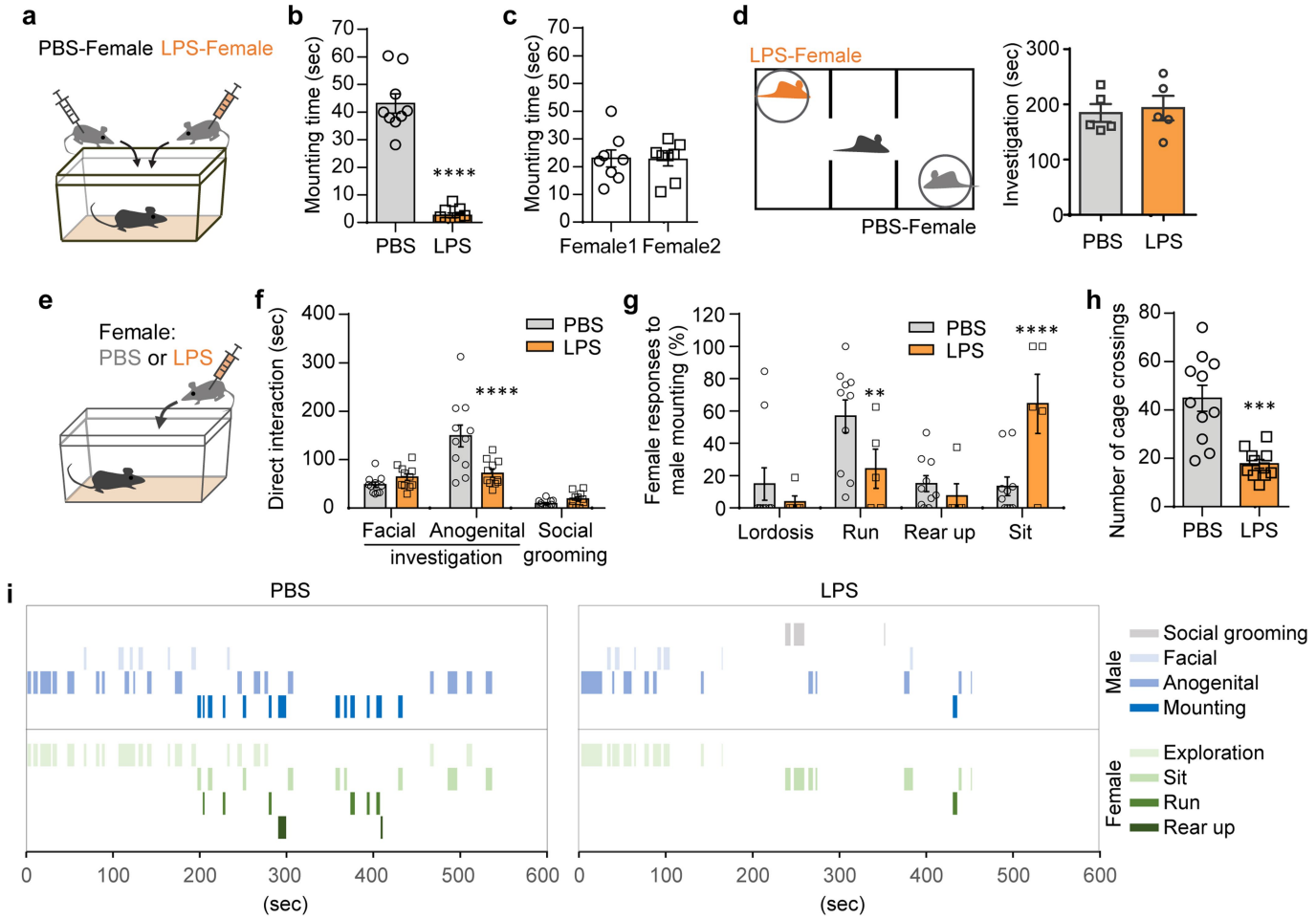

Extended Data Fig. 1 | Male mice avoid mounting sick females. a, **b**, Male mice were presented with a pair of oestrus female mice each injected intraperitoneally with either PBS (PBS female) or LPS (LPS female) (**a**). Mounting time during a 10-min test (**b**) ($n = 9$; from 2 independent experiments). **c**, Mounting time for male mice presented with two untreated, healthy females ($n = 8$; from 2 independent experiments). **d**, Investigation time of PBS and LPS females during a 10-min three-chamber assay ($n = 5$; from 2 independent experiments). **e**–**i**, These data are associated with Fig. 1a–e. Duration of other typical male behaviours while engaged in direct interactions with a PBS or LPS female (**e**, **f**). Percentage of individual female behaviours during males' mounting attempts (**g**) and the number of cage crossings (**h**). Representative traces of male and female behaviours during direct interactions (**i**). $^{**}P < 0.01$, $^{***}P < 0.001$ and $^{****}P < 0.0001$ calculated by paired two-tailed *t*-test (**b**), two-way ANOVA with Sidak's post hoc test (**f**, **g**) and unpaired two-tailed *t*-test (**h**). Data are mean ± s.e.m. *P* values are described in the Supplementary Statistical Information.

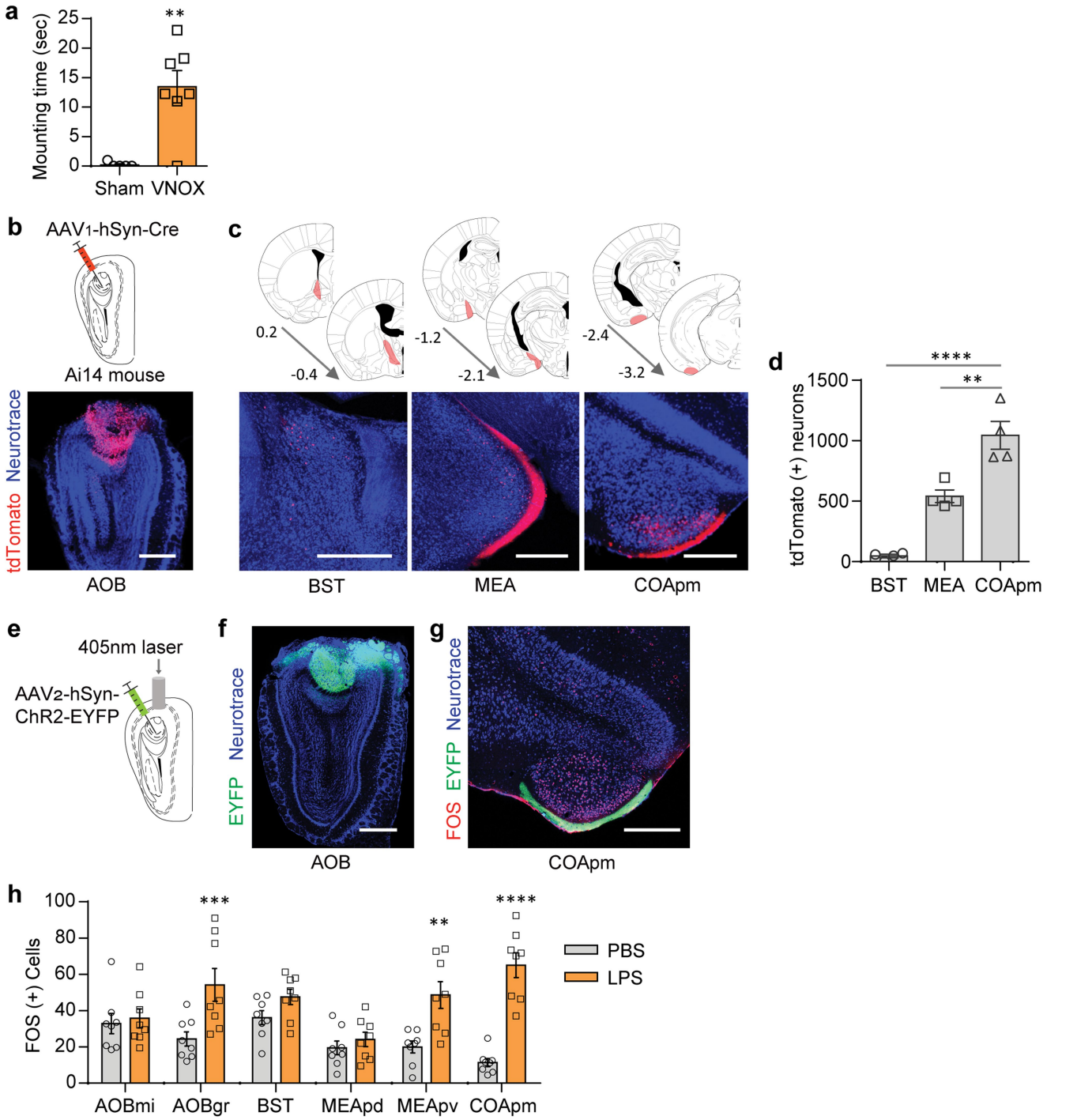

Extended Data Fig. 2 | Role of the vomeronasal pathway in mounting behaviour. a, Mounting time for males with a sham surgery (sham) or the VNO removed (VNOX) towards LPS females (sham, $n = 5$ and VNOX, $n = 7$; from 2 independent experiments). **b**–**d**, Virus encoding the anterograde trans-synaptic tracer (AAV_1-hSyn-Cre) was targeted to the AOB in Ai14 reporter mice that express tdTomato in a Cre-dependent manner (**b**). Representative images (**c**) and quantification (**d**) of trans-synaptically labelled tdTomato$^+$ neurons in BST, MEA and COApm at the specified anterior-posterior axis ($n = 4$; from 3 independent experiments). Scale bars, 500 µm. **e**–**g**, Virus encoding ChR2 (AAV_2-hSyn-hChR2-eYFP) was targeted to the AOB (**e**, **f**). **g**, Representative image of FOS expression in the COApm upon photoactivation of the AOB, from $n = 3$ mice. Scale bars, 500 µm. **h**, These data are associated with Fig. 1g. Number of FOS-expressing neurons in the vomeronasal pathway after interaction with PBS or LPS females. $^{**}P < 0.01$, $^{***}P < 0.001$ and $^{****}P < 0.0001$ calculated by unpaired two-tailed *t*-test (**a**), one-way ANOVA with Bonferroni's post hoc test (**d**) and two-way ANOVA with Sidak's post hoc test (**h**). Graph indicates mean ± s.e.m. *P* values are described in the Supplementary Statistical Information.

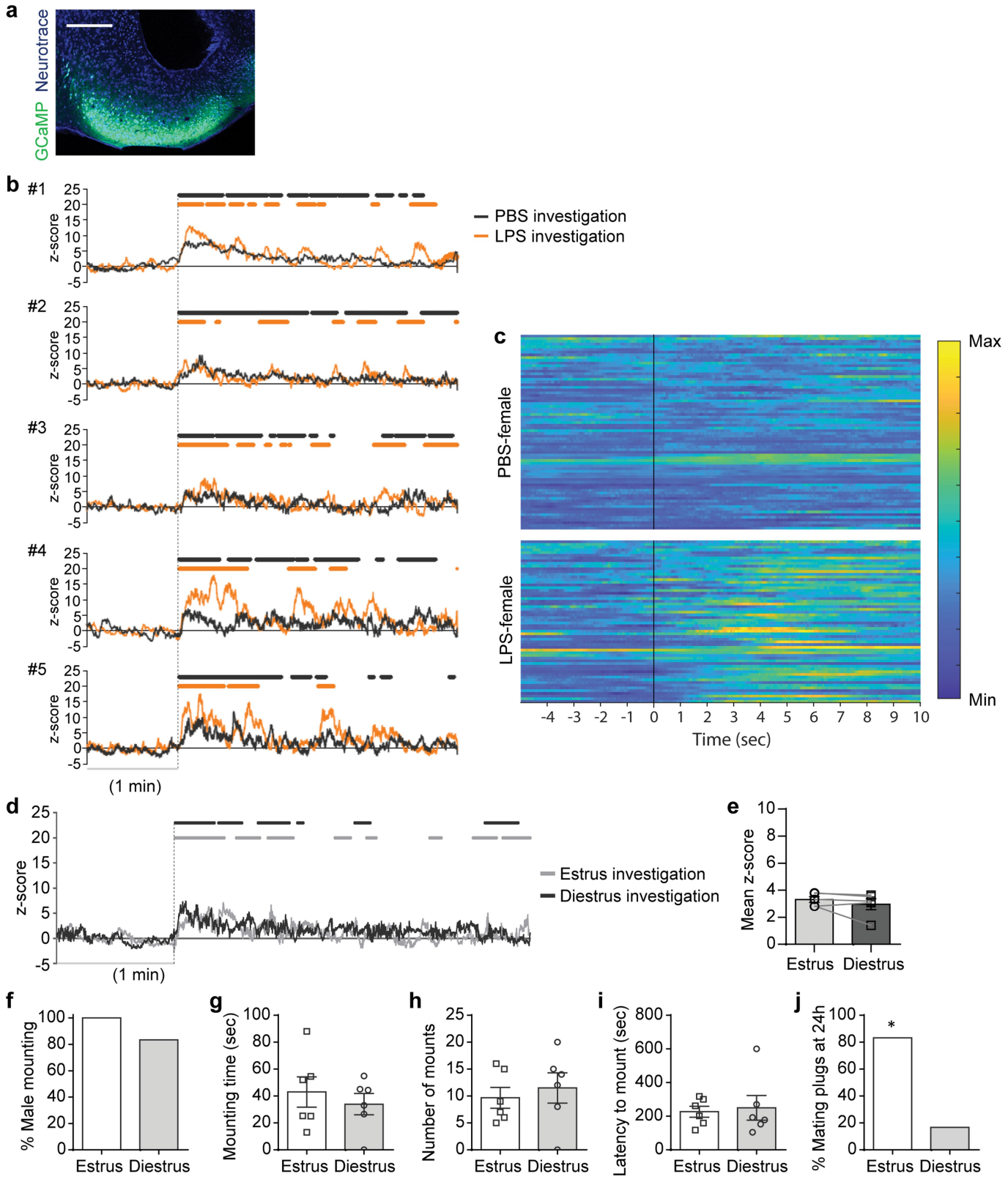

Extended Data Fig. 3 | See next page for caption.

Extended Data Fig. 3 | Investigation of LPS females induces neural activity in the COApm of males. a–**c**, These data are associated with Fig. 1h–o. **a**, Representative image of GCaMP6s expression in the COApm. Scale bar, 300 µm. **b**, Individual traces of COApm bulk fluorescence signal during interactions with a PBS or LPS female. **c**, Heat map of normalized COApm responses to PBS or LPS females. Each row represents a single investigation event. Investigation events were pooled from 6 mice from 3 independent experiments. Time = 0 indicates initiation of investigation. **d**, **e**, Virus encoding GCaMP6s (AAV_1-Syn-GCaMP6s) was targeted to the COApm for fibre photometry recordings. Male mice were sequentially presented with an oestrus or dioestrus female in counterbalanced sessions. Representative traces of COApm bulk fluorescence signal (**d**) and the mean *z*-score of the fluorescence during direct investigation of the oestrus or dioestrus female (**e**) (oestrus, $n = 5$ and dioestrus, $n = 5$; from 3 independent experiments). **f**–**j**, Male mounting behaviours towards an oestrus or dioestrus, healthy female. Percentage of male mounting (**f**), mounting time (**g**), number of mounts (**h**), latency to mount (**i**) and percentage of female partners with mating plugs (**j**) (oestrus, $n = 6$ and dioestrus, $n = 6$; from 2 independent experiments). **j**, $^*P < 0.05$ calculated by chi-square test of independence. Data are mean ± s.e.m. *P* values are described in the Supplementary Statistical Information.

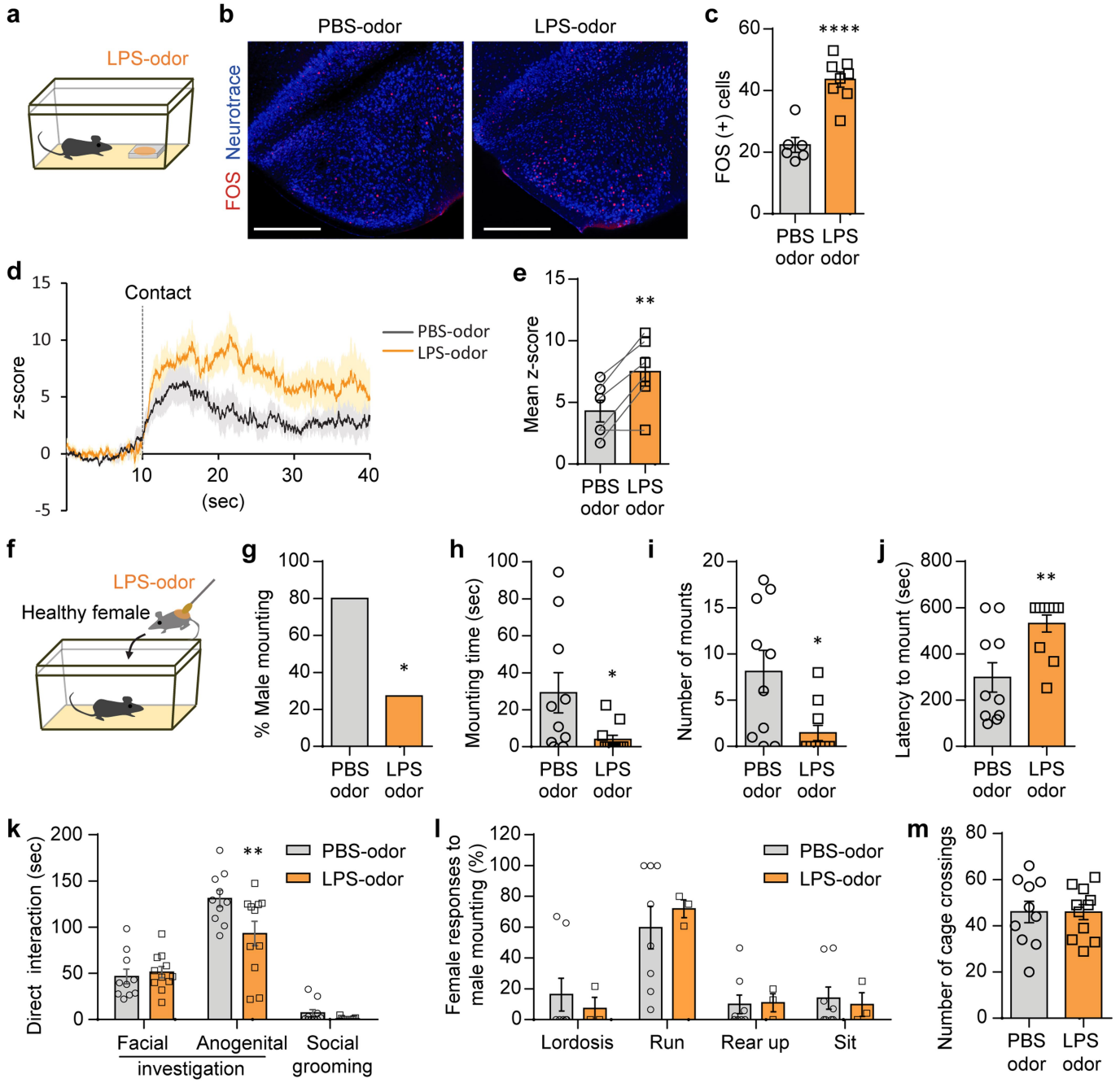

Extended Data Fig. 4 | LPS odour suppresses male mating behaviours. **a**–**c**, Male mice were presented with PBS or LPS odour (**a**). Representative images (**b**) and quantification (**c**) of FOS expression in the COApm of males after exposure to PBS or LPS odour (PBS odour, $n = 6$ and LPS odour, $n = 8$; from 2 independent experiments). Scale bar, 500 µm. **d**, **e**, Virus encoding GCaMP6s (AAV_1-Syn-GCaMP6s) was targeted to the COApm for fibre photometry recordings. Male mice were sequentially presented with a PBS or LPS odour in counterbalanced sessions. Traces of COApm bulk fluorescence signal (solid line shows the average and shaded area indicates the s.e.m.) (**d**) and the mean *z*-score of the fluorescence during the first 20 s of direct investigation of the odour (**e**) ($n = 6$; from 3 independent experiments). **f**–**m**, Male mice were presented with a healthy female painted with PBS or LPS odour (**f**). Percentage of male mounting (**g**), mounting time (**h**), number of mounts (**i**), latency to mount (**j**) and duration of additional male behaviours while engaged in direct interactions with the female (**k**). Percentage of female behaviours in response to males' mounting attempts (**l**) and the number of cage crossings (**m**) (PBS odour, $n = 10$ and LPS odour, $n = 11$; from 2 independent experiments). $^*P < 0.05$, $^{**}P < 0.01$ and $^{****}P < 0.0001$ calculated by unpaired two-tailed *t*-test (**c**, **h**–**j**), paired two-tailed *t*-test (**e**), chi-square test of independence (**g**) and two-way ANOVA with Sidak's post hoc test (**k**). Data are mean ± s.e.m. *P* values are described in the Supplementary Statistical Information.

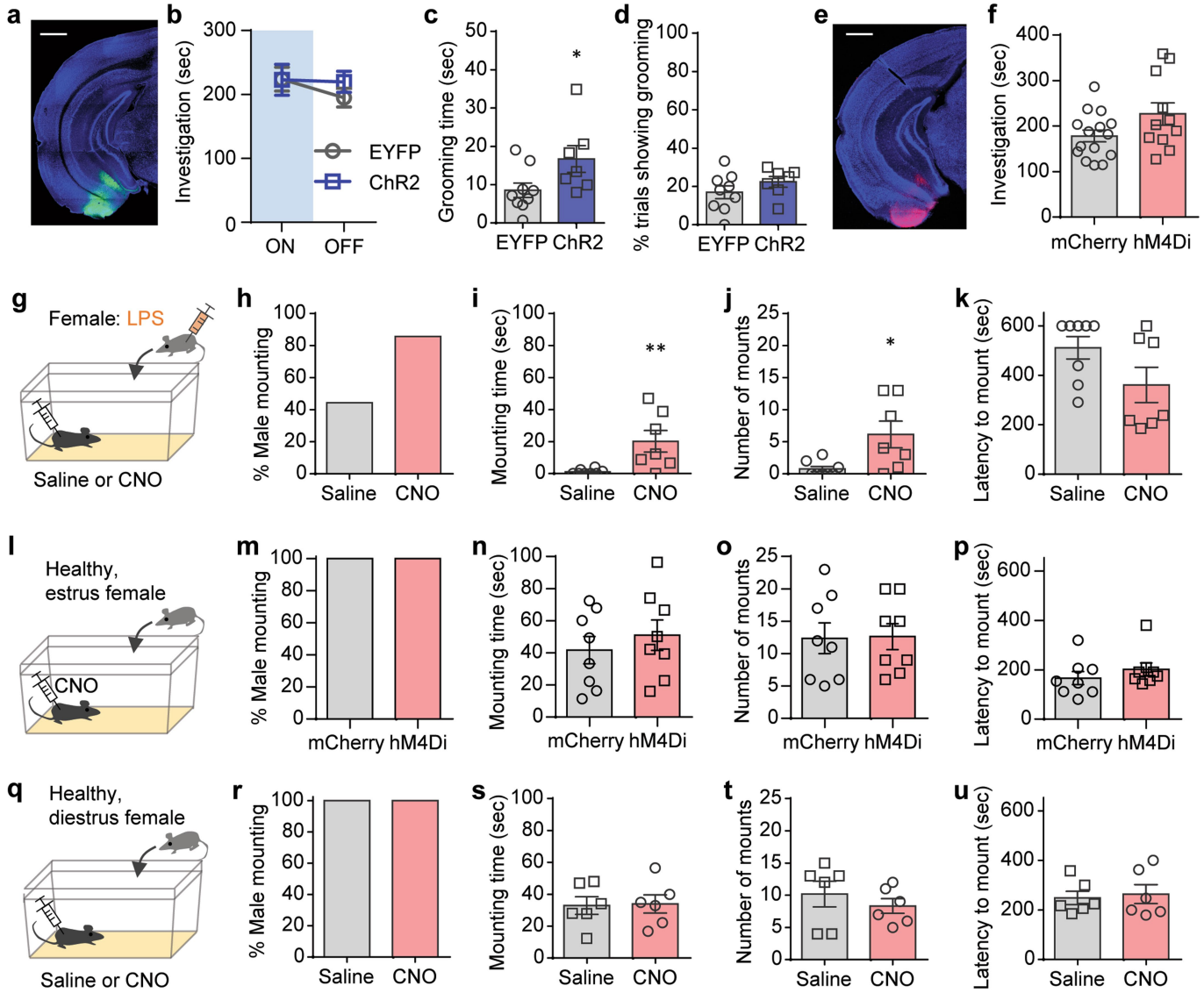

Extended Data Fig. 5 | COApm mediates suppression of mating behaviours towards unhealthy females. a–d, These data are associated with Fig. 2a–e. **a**, Representative image of ChR2 expression in the COApm. **b**, Total direct investigation time of healthy females in the presence (ON) and absence (OFF) of COApm photoactivation. Duration of self grooming (**c**) and percentage of photoactivation trials with self grooming (**d**). Scale bar, 1 mm. **e**, **f**, These data are associated with Fig. 2i–m. Representative image of hM4Di expression in the COApm (**e**) and total direct investigation time of LPS females (**f**). Scale bar, 1 mm. **g–k**, Additional control experiments for data in Fig. 2i–m. Male mice expressing inhibitory DREADD (AAV_2-hSyn-hM4D(G_i)-mCherry) in COApm were injected with either saline or CNO and tested for mounting behaviour towards LPS females (**g**). Percentage of male mounting (**h**), mounting time (**i**), number of mounts (**j**) and latency to mount (**k**) (saline, $n = 8$ and CNO, $n = 7$; from 2 independent experiments). **l–p**, Male mice expressing mCherry (AAV_2-hSyn-mCherry) or inhibitory DREADD (hM4Di, AAV_2-hSyn-hM4D(G_i)-mCherry) in COApm were injected with CNO and tested for mounting behaviour towards untreated, healthy oestrus females (**l**). Percentage of male mounting (**m**), mounting time (**n**), number of mounts (**o**) and latency to mount (**p**) (mCherry, $n = 8$ and hM4Di, $n = 8$; from 2 independent experiments). **q–u**, Male mice expressing inhibitory DREADD (AAV_2-hSyn-hM4D(G_i)-mCherry) in COApm were injected with saline or CNO and tested for mounting behaviour towards untreated, healthy dioestrus females (**q**). Percentage of male mounting (**r**), mounting time (**s**), number of mounts (**t**), and latency to mount (**u**) (saline, $n = 6$ and CNO, $n = 6$; from 2 independent experiments). $^*P < 0.05$, $^{**}P < 0.01$ calculated by unpaired two-tailed *t*-test (**c**, **i**, **j**). Data are mean ± s.e.m. P values are described in the Supplementary Statistical Informatio.

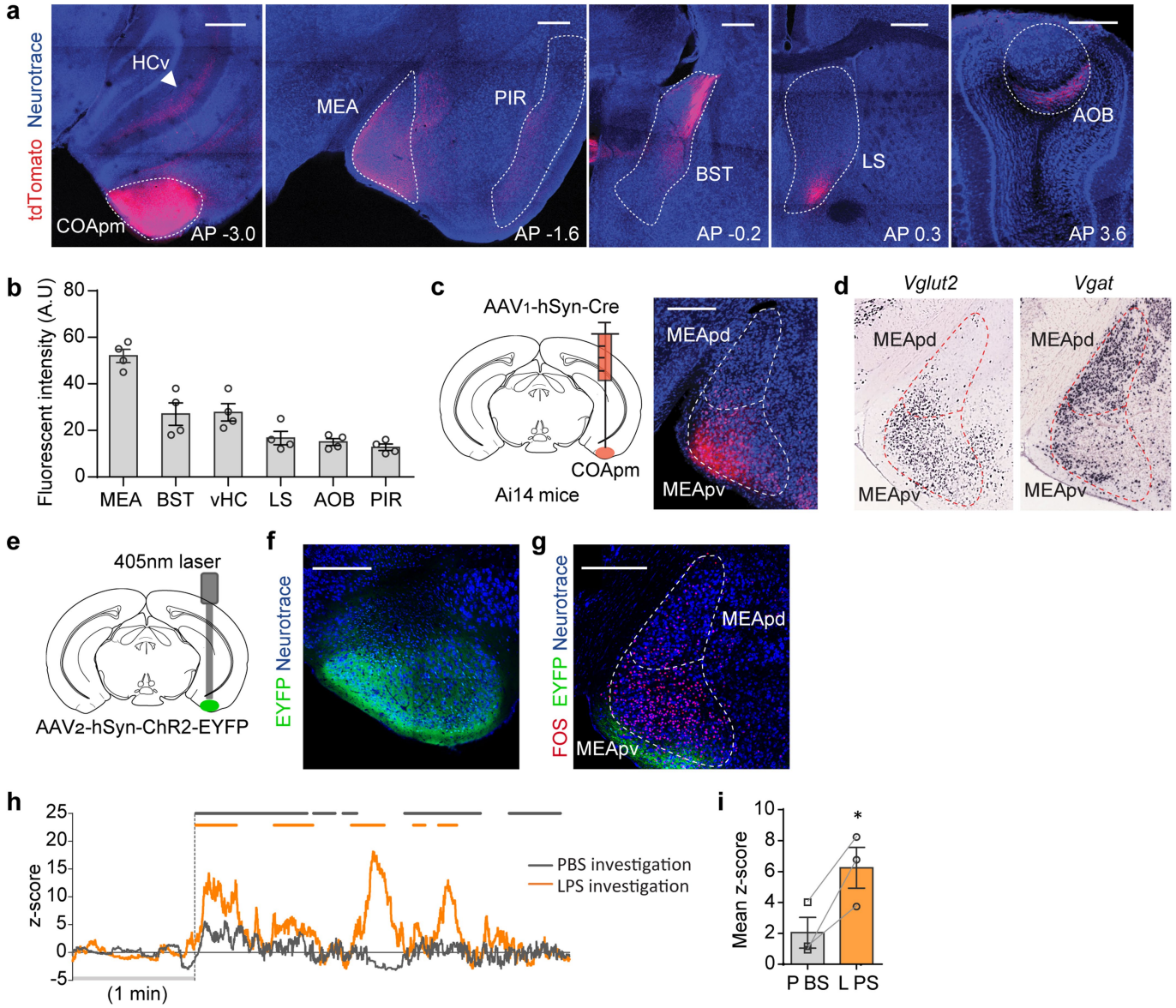

Extended Data Fig. 6 | COApm neurons preferentially project to MEA-Vglut2$^+$ neurons. a, **b**, Virus encoding the anterograde tracer (AAV_2-hSyn-tdTomato) was targeted to the COApm. Total fluorescence intensity was measured in sub-regions receiving COApm axonal projections: MEA, BST, ventral hippocampus (HCv), lateral septum (LS), AOB and piriform cortex (PIR) ($n = 4$ mice; from 2 independent experiments). Scale bars, 500 µm. **c**, Virus encoding the anterograde trans-synaptic tracer (AAV_1-hSyn-Cre) was targeted to the COApm of Ai14 reporter mice that express tdTomato in a Cre-dependent manner. Representative image of MEA post-synaptic neurons at AP −1.7 mm, from 3 independent experiments. Scale bar, 300 µm. **d**, mRNA expression of *Vglut2* and *Vgat* in MEA (Image credit: Allen Institute). **e**–**g**, ChR2 (AAV_2-hSyn-ChR2-eYFP) was targeted to the COApm (**e**). Representative images of ChR2 expression in COApm (**f**) and FOS expression in MEA upon photoactivation of COApm (**g**) ($n = 3$; from 2 independent experiments). Scale bars, 300 µm. **h**, **i**, Virus encoding GCaMP6s (AAV_1-Syn-GCaMP6s) was targeted to the MEA of Vglut2-Cre mice for fibre photometry recordings. Male mice were sequentially presented with a PBS or LPS female in counterbalanced sessions. Representative traces of MEA-vGlut2$^+$ bulk fluorescence signal (**h**) and the mean *z*-score of the fluorescence during direct investigation of the PBS or LPS female (**i**) ($n = 3$; from 2 independent experiments). **i**, $^*P < 0.05$ calculated by paired two-tailed *t*-test. Data are mean ± s.e.m. *P* values are described in the Supplementary Statistical Information.

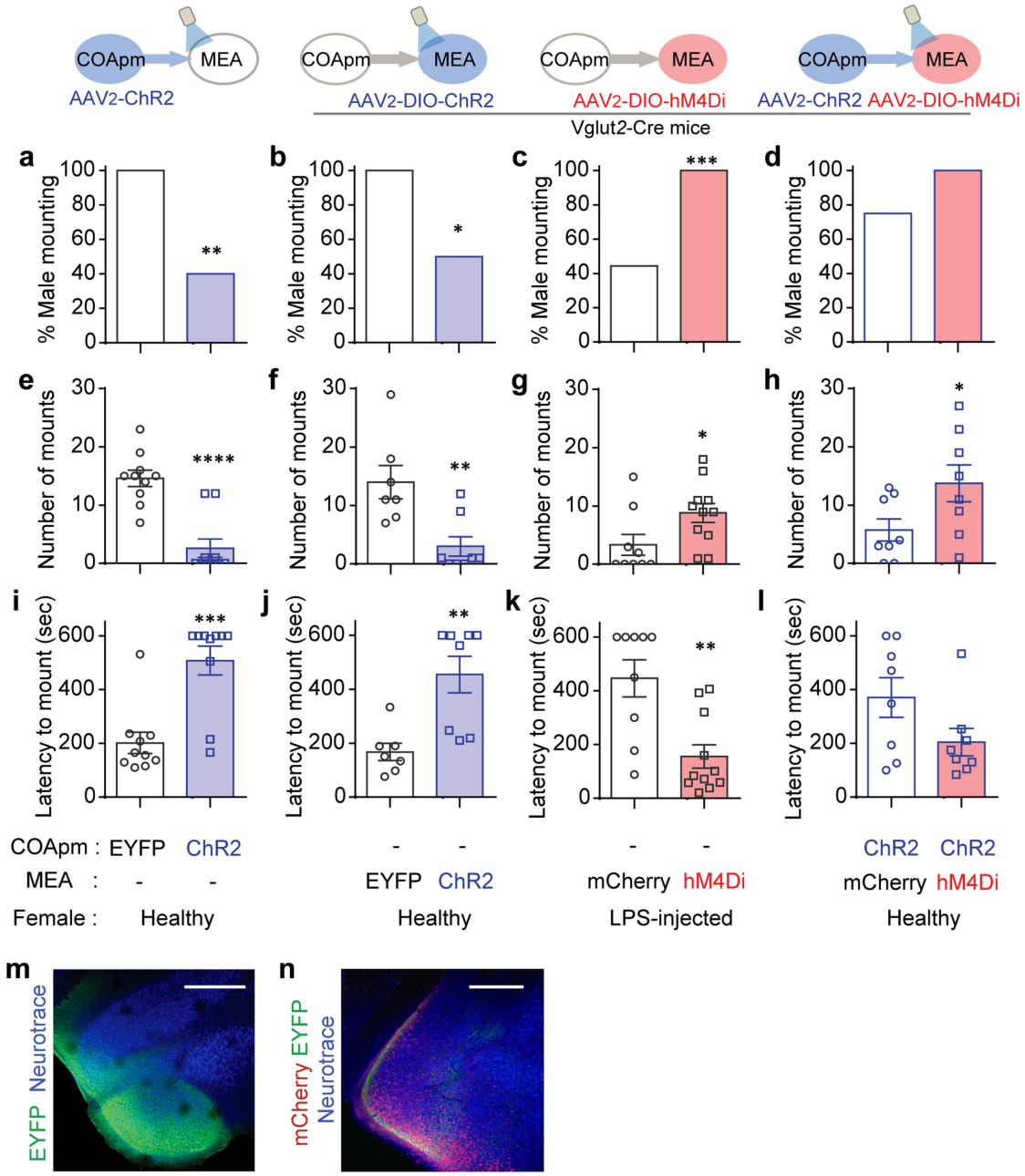

Extended Data Fig. 7 | COApm suppresses male mating behaviours by engaging MEA-Vglut2$^+$ neurons. These data are associated with Fig. 3f–i. Percentage of male mounting (**a**–**d**), number of mounts (**e**–**h**), latency to mount (**i**–**l**). Representative images of ChR2 expression in COApm (**m**) and hM4Di expression in MEA (**n**) of Vglut2-Cre mice with concurrent photoactivation of COApm-MEA projections and hM4Di-inhibition of MEA-Vglut2$^+$ neurons. Scale bars, 500 µm. *P < 0.05, **P < 0.01, ***P < 0.001 and ****P < 0.0001 calculated by chi-square test of independence (**a**–**c**) and unpaired two-tailed t-test (**e**–**k**). Data are mean ± s.e.m. P values are described in the Supplementary Statistical Information.

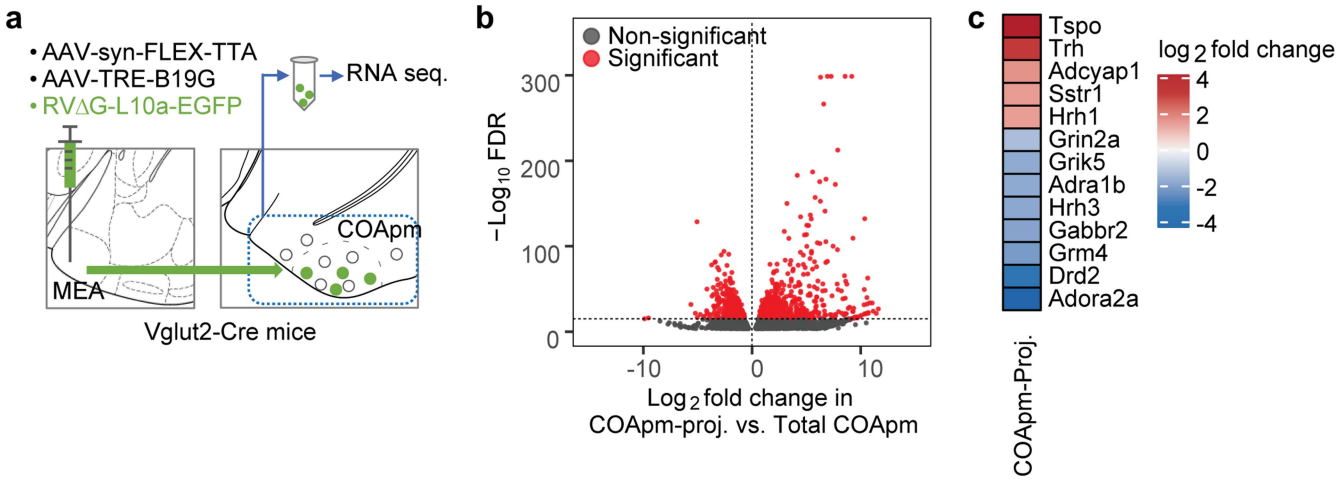

Extended Data Fig. 8 | Summary of gene-expression profiling in COApm neurons projecting to MEA-Vglut2$^+$ neurons. a, A combination of AAV_1-Syn-FLEX-TTA and AAV-TRE-B19G, and RVΔG-L10a-eGFP were sequentially injected into the MEA of Vglut2-Cre mice to express L10a-eGFP in COApm neurons projecting to MEA-Vglut2$^+$ neurons (COApm-proj). COApm tissue was collected and immediately used for TRAP analyses. Control mice were injected with AAV.PHP.eB-Syn-L10a-eGFP via retro-orbital injection in order to label COApm neurons with L10a-eGFP independently of their efferent projections (Total COApm). **b**, Volcano plot showing log_2-fold change plotted against $-log_{10}$ FDR for the labelled COApm neurons projecting to the MEA-Vglut2$^+$ population (COApm-Proj.) compared to the total COApm. Differentially expressed genes that pass the threshold for the FDR are highlighted in red. **c**, Heat map showing COApm-differentially expressed genes that belong to the KEGG neuroactive ligand–receptor interaction pathway. *P* values are described in the Supplementary Statistical Information.

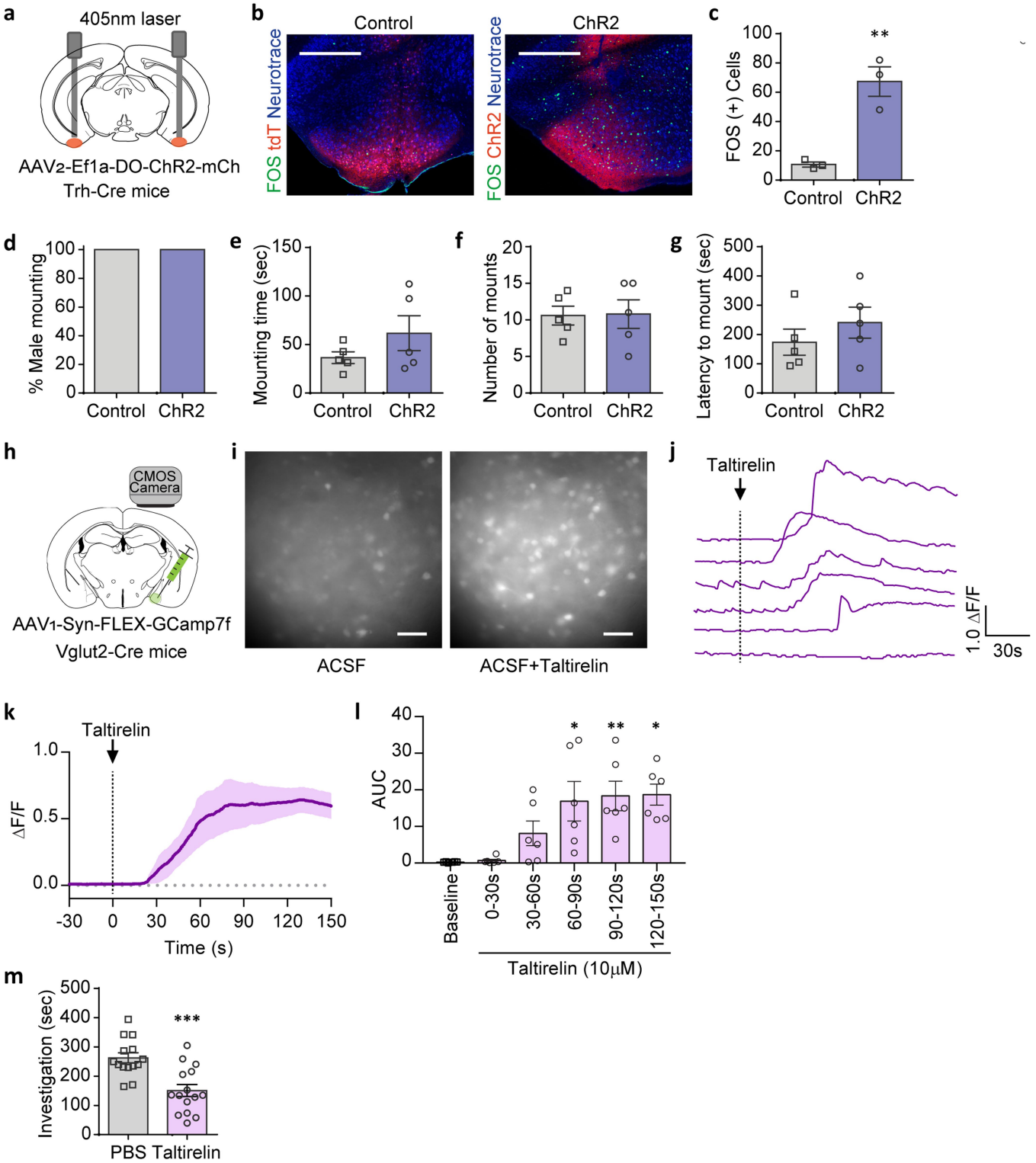

Extended Data Fig. 9 | COApm-TRH$^+$ neurons mediate the suppression of male mating towards unhealthy females. a–**g**, Trh-Cre male mice expressing tdTomato ($AAV_{1/2}$-Ef1α-DO-DIO-tdTomato(tdT)-eGFP, Control) or ChR2 ($AAV_{1/2}$-Ef1α-DO-ChR2-mCherry, ChR2) in Cre$^-$ neurons were tested for mating behaviours towards healthy females with COApm photoactivation (**a**). Representative images (**b**) and quantification (**c**) of FOS expression in COApm. Percentage of male mounting (**d**), mounting time (**e**), number of mounts (**f**), and latency to mount (**g**) with photoactivation of COApm-TRH$^-$ cells (control, $n = 5$ and ChR2, $n = 5$; from 2 independent experiments). Scale bars, 500 μm. **h**–**l**, Calcium imaging of MEA brain slices from Vglut2-Cre mice expressing GCaMP7f (AAV_1-hSyn-FLEX-GCaMP7f) in MEA-Vglut2$^+$ neurons upon taltirelin (10 μM) application (**h**). **i**, Representative images of MEA slices before (−15 s) and after (+35 s) taltirelin application. Example traces of fluorescence signal from individual neurons (**j**) and the average of the fluorescence signal (solid line shows average and shaded area represents the s.e.m.) (**k**) upon taltirelin application. **l**, Area under the curve (AUC) of the average fluorescence signal from individual MEA slices binned every 30 s ($n = 6$ slices, from 3 mice). Scale bars, 50 μm. **m**, These data are associated with Fig. 4k–o. Total duration of direct investigation following microinjection of the TRH analogue taltirelin into MEA. $^*P < 0.05$, $^{**}P < 0.01$ and $^{***}P < 0.001$ calculated by unpaired two-tailed *t*-test (**c**, **m**) and Friedman test with Dunn's multiple comparisons test (**l**). Data are mean ± s.e.m. *P* values are described in the Supplementary Statistical Information.

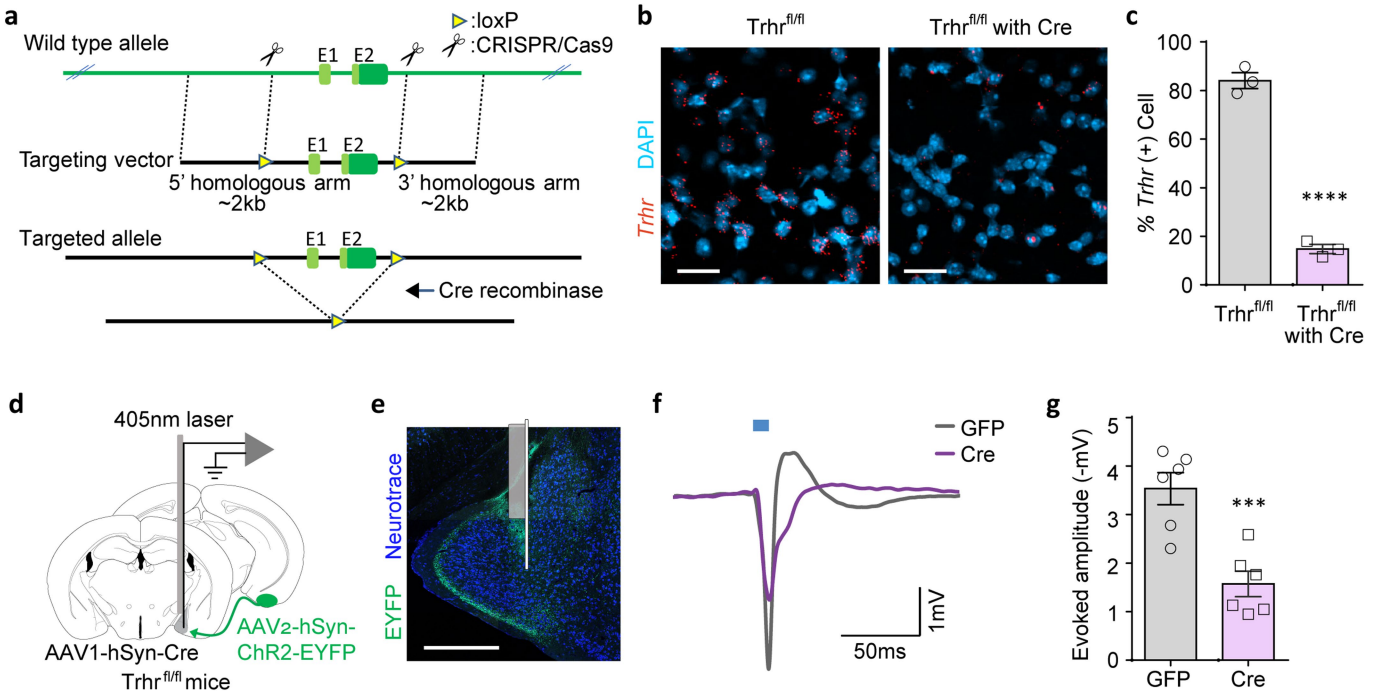

Extended Data Fig. 10 | Suppression of mating engages TRH–TRHR signalling in the COApm-MEA projection. a, Schematic depicting the targeting construct used to generate the *Trhr* conditional-knockout mouse line. **b**, **c**, Representative images (AP −1.8 mm) (**b**) and quantification (**c**) of *Trhr* mRNA expression in the MEApv of $Trhr^{fl/fl}$ mice with or without Cre expression (AAV_1-hSyn-Cre) ($Trhr^{fl/fl}$, $n = 3$ and $Trhr^{fl/fl}$ with Cre, $n = 3$; from 2 independent experiments). Scale bars, 20 µm. **d**–**g**, In vivo recordings of MEA responses to COApm inputs in Trhr conditional-knockout mice. $Trhr^{fl/fl}$ mice were injected with AAV_2-hSyn-ChR2-eYFP in COApm and either AAV_1-hSyn-GFP (GFP) or AAV_1-hSyn-Cre (Cre) in MEApv. **d**, Local field potentials evoked by a 10-ms photoactivation were recorded from MEApv in anaesthetized mice using an optrode. **e**, Representative image of electrode localization. Representative waveforms (**f**) and amplitudes (baseline-to-negative peak) of MEApv responses evoked by photoactivation of COApm inputs (**g**) (GFP, $n = 6$ and Cre, $n = 6$; from 6 independent experiments). Scale bar, 300 µm. $^{***}P < 0.001$ and $^{****}P < 0.0001$ calculated by unpaired two-tailed *t*-test (**c**, **g**). Data are mean ± s.e.m. *P* values are described in the Supplementary Statistical Information.

nature research

Corresponding author(s): Gloria B. Choi

Last updated by author(s): 02/23/2021

Reporting Summary

Nature Research wishes to improve the reproducibility of the work that we publish. This form provides structure for consistency and transparency in reporting. For further information on Nature Research policies, see Authors & Referees and the Editorial Policy Checklist.

Statistics

For all statistical analyses, confirm that the following items are present in the figure legend, table legend, main text, or Methods section.

n/a	Confirmed
☐	☒ The exact sample size (*n*) for each experimental group/condition, given as a discrete number and unit of measurement
☐	☒ A statement on whether measurements were taken from distinct samples or whether the same sample was measured repeatedly
☐	☒ The statistical test(s) used AND whether they are one- or two-sided *Only common tests should be described solely by name; describe more complex techniques in the Methods section.*
☐	☒ A description of all covariates tested
☐	☒ A description of any assumptions or corrections, such as tests of normality and adjustment for multiple comparisons
☐	☒ A full description of the statistical parameters including central tendency (e.g. means) or other basic estimates (e.g. regression coefficient) AND variation (e.g. standard deviation) or associated estimates of uncertainty (e.g. confidence intervals)
☐	☒ For null hypothesis testing, the test statistic (e.g. *F*, *t*, *r*) with confidence intervals, effect sizes, degrees of freedom and *P* value noted *Give P values as exact values whenever suitable.*
☒	☐ For Bayesian analysis, information on the choice of priors and Markov chain Monte Carlo settings
☒	☐ For hierarchical and complex designs, identification of the appropriate level for tests and full reporting of outcomes
☐	☒ Estimates of effect sizes (e.g. Cohen's *d*, Pearson's *r*), indicating how they were calculated

Our web collection on statistics for biologists contains articles on many of the points above.

Software and code

Policy information about availability of computer code

Data collection	Behavioral experiments were recorded using Ethovision XT. Fiber photometry signals were processed by custom LabVIEW 2015 software. mRNA expressions were quantified using QuPath (v.0.1.2). Images of calcium imaging in brain slices were acquired using Micro-manager(v2.0.0-gamma1) and further processed with EZcalcium open-source MATLAB toolbox. Confocal images were acquired and analyzed using ZEN3.0.
Data analysis	Data were analyzed using Graphpad Prism v8.0.1.

For manuscripts utilizing custom algorithms or software that are central to the research but not yet described in published literature, software must be made available to editors/reviewers. We strongly encourage code deposition in a community repository (e.g. GitHub). See the Nature Research guidelines for submitting code & software for further information.

Data

Policy information about availability of data

All manuscripts must include a data availability statement. This statement should provide the following information, where applicable:

- Accession codes, unique identifiers, or web links for publicly available datasets
- A list of figures that have associated raw data
- A description of any restrictions on data availability

Source data containing raw data for experiments are provided with the paper. RNA sequencing data are available in NCBI under accession #GSE167176. All other data are available from the corresponding author upon request.

Field-specific reporting

Please select the one below that is the best fit for your research. If you are not sure, read the appropriate sections before making your selection.

☒ Life sciences ☐ Behavioural & social sciences ☐ Ecological, evolutionary & environmental sciences

For a reference copy of the document with all sections, see nature.com/documents/nr-reporting-summary-flat.pdf

Life sciences study design

All studies must disclose on these points even when the disclosure is negative.

Sample size	Sample size was chosen based on similar previous studies (reference 24,49).
Data exclusions	Behavioral results from mice with inaccurate targeting of viral infection (Fig.2 and Fig.3f-i) or cannula implantations (Fig.4k) were excluded. For fiber photometry experiments, mice with low fluorescence signal below our criteria were excluded for further analysis as described in method section.
Replication	Key experiments were verified with more than two independent experiments. All attempts at replication were successful.
Randomization	Animals were randomly assigned to groups with approximately balanced sample size.
Blinding	Experimenters were blind to subject treatment during data collection and analysis.

Reporting for specific materials, systems and methods

We require information from authors about some types of materials, experimental systems and methods used in many studies. Here, indicate whether each material, system or method listed is relevant to your study. If you are not sure if a list item applies to your research, read the appropriate section before selecting a response.

Materials & experimental systems

n/a	Involved in the study
☐	☒ Antibodies
☐	☒ Eukaryotic cell lines
☒	☐ Palaeontology
☐	☒ Animals and other organisms
☒	☐ Human research participants
☒	☐ Clinical data

Methods

n/a	Involved in the study
☒	☐ ChIP-seq
☒	☐ Flow cytometry
☒	☐ MRI-based neuroimaging

Antibodies

Antibodies used	Rabbit anti-FOS (1:500, Millipore, ABE457), Alexa 488 Goat anti-rabbit (1:250, Life Technologies, A11034), Biotin-linked mouse anti-GFP antibody (custom made, clones 19F7 and 19C8, concentration: 50ug of 19F7 and 19C8 for each IP)
Validation	All primary antibodies have been used and validated in previous publications.

Eukaryotic cell lines

Policy information about cell lines

Cell line source(s)	HEK293FT cell (ThermoFisher)
Authentication	The cell line was authenticated by vendor
Mycoplasma contamination	The cell line was not contaminated by mycoplasma as determined by qPCR Assay
Commonly misidentified lines (See ICLAC register)	No commonly misidentified lines were used

Animals and other organisms

Policy information about studies involving animals; ARRIVE guidelines recommended for reporting animal research

Laboratory animals	WT male mice used for experiments were C57BL/6 mice. 2-5 months old male Ai14, Trh-Cre, Trhr-Cre, Vglut2-Cre, and Vgat-Cre mice in the C57BL/6 background were also used for experiments. 2-3 months old female C57BL/6 mice were used for mating test. Sources for all mice used are reported in the methods.
Wild animals	Study did not involve wild animals.
Field-collected samples	Study did not involve field-collected samples
Ethics oversight	Committee on Animal Care at Harvard Medical School and Massachusetts Institute of Technology provided approval for all experiments.

Note that full information on the approval of the study protocol must also be provided in the manuscript.